Journal Pre-proofs

Altered electrochemistry of poly(3,4-ethylenedioxythiophene) after activation of the inserted cobalt ions

Esteban Guillén-Bas, Jerónimo Agrisuelas, José J. García-Jareño, Francisco Vicente

Please cite this article as: E. Guillén-Bas, J. Agrisuelas, J.J. García-Jareño, F. Vicente, Altered electrochemistry of poly(3,4-ethylenedioxythiophene) after activation of the inserted cobalt ions, *Journal of Electroanalytical Chemistry* (2024), doi: https://doi.org/10.1016/j.jelechem.2024.118440

This is a PDF file of an article that has undergone enhancements after acceptance, such as the addition of a cover page and metadata, and formatting for readability, but it is not yet the definitive version of record. This version will undergo additional copyediting, typesetting and review before it is published in its final form, but we are providing this version to give early visibility of the article. Please note that, during the production process, errors may be discovered which could affect the content, and all legal disclaimers that apply to the journal pertain.

Altered electrochemistry of poly(3,4-ethylenedioxythiophene) after activation of the inserted cobalt ions

Esteban Guillén-Bas[a,b] *, Jerónimo Agrisuelas[a], José J. García-Jareño[a], and Francisco Vicente[a]

[a]Departament de Química Física, Universitat de València. C/ Dr. Moliner, 50, 46100, Burjassot, València, Spain.

[b] Departament de Química Inorgànica, Universitat d'Alacant. Carretera de San Vicente s/n, 03690, Alacant, Spain.

* E-mail: esteban.guillen@ua.es

HIGHLIGTHS

- Synthesis of PEDOT in aqueous solutions by chronoamperometry.
- Cobalt incorporation inside PEDOT by cyclic voltammetry
- Activation of inserted cobalt by lithium incorporation
- PEDOT(aCo) characterization by hyphenated techniques

ABSTRACT

Cobalt ions were inserted into poly(3,4-ethylenedioxythiophene) by cyclic voltammetry in a 0.1M $Co(NO_3)_2$ aqueous solution (PEDOT(Co)). After activation of the inserted cobalt, the PEDOT(aCo) system was investigated by cyclic voltammetry, digital video electrochemistry, spectroelectrogravimetry, and coupled impedance techniques (ac-electrogravimetry) to elucidate the key role of inserted cobalt ions in the altered electrochemistry of PEDOT. The incorporation of Co^{2+} involves slow transfer of cations for charge compensation during $Co^{2+} \rightleftarrows Co^{3+}$ conversion inside the PEDOT. This fact explains the enhanced charge storage showed by PEDOT(aCo) compared with pristine PEDOT at similar potentials. Finally, the stability of PEDOT(aCo) was investigated by cyclic voltammetry measuring at the same time current, mass and motional resistance variation during 100 cycles offering high stability at all times.

1.   INTRODUCTION

Nowadays, energy capture and storage have become critical topics in our society. Consequently, the scientific community faces a challenge from society to develop new materials or devices that can meet the growing energy demand [1–4]. Supercapacitors are shown promise for energy storage, with their high specific power, long cycle life, fast charge rate, high safety, and ease of manufacture [3]. As a result, their use has increased significantly in areas such as portable electronics, backup power supply, regenerative braking systems, motor starter devices, and large-scale industrial power and energy management [5,6].

Supercapacitors are generally categorized into two primary types based on their charge storage [1,7,8]. The first type is the electrical double-layer capacitor, where the double-layer capacitance arises at the electrode|electrolyte interface. Typical carbon-based materials are commonly used as electrodes in electrical double-layer capacitors because of their high surface area and excellent stability. However, they have a low specific capacitance. The second type is pseudo-capacitors, where pseudo-capacitance arises from rapid surface redox reactions. Metal oxides and conducting polymers are commonly used as electrode materials in pseudo-capacitors. Conducting polymers (CPs) provide additional functionalities to create smart supercapacitors with properties such as electrochromism, electrochemical actuation, stretchability, self-healing, and stimuli-sensitive properties [9].

At the molecular level, the electrochemical oxidation and reduction processes of CPs involve the creations and destruction of polymer charged sites (polarons and/or bipolarons), which accommodates ions to keep the electroneutrality together with solvent molecules. Occasionally, these electrochemical processes are accompanied by color changes, which provide qualitative information about the energy level of the supercapacitor [10–12]. This information is possible by the in situ combination of electrochemical techniques with spectroscopy, gravimetry and/or motional resistance measurements, which have been successfully used in recent years to study of electrochemical processes in CPs [13–22]. The in situ techniques can help to elucidate the molecular mass of the involved species and/or the separation of overlapped reactions [23–26]. Measurements of the viscoelastic changes with the motional resistance during the doping-dedoping of films is essential to know the future structural integrity of the supercapacitor device based on conducting polymers [20]. Electrochemical techniques working in the frequency domain allow to explore the kinetics, charge transport mechanisms and the role of anions, cation and solvent in the electrochemical processes of CPs [27–29].

The synthesis of most of conducting polymers is widely studied, and these materials often exhibit high specific capacitance and some stability [2]. Among the most extensively researched CPs, the poly(3,4-ethylendioxythiophene) (PEDOT) has good conductivity, easy processability, and high stability [30–36]. PEDOT has a rigid and linear conformation which facilitates the electronic and ion transport to keep the charge balance inside the film [37–44]. These characteristics leads to high charge/discharge cycles [39,45]. Incorporating transition metal oxides into CPs results in synergistic effects on the supercapacitor performance. Electrodes of Co_3O_4 favors fast redox reaction and high value of specific capacitance in supercapacitors and lithium ion batteries due to the multiple oxidation states of cobalt ions [46–54]. Recently, some authors demonstrated that integrating Co_3O_4 into highly conductive polymers improved the specific

4

capacitances and capacitance retentions [55–59]. However, the low conductivity and poor surface area of Co_3O_4 have limited its applications [60]. Only a few studies have focused on incorporating cobalt ions into the PEDOT films and examining their electrochemical processes [61]. This is why in this work we have studied the electrochemical insertion of cobalt into the polymeric matrix.

The insertion of transition metal compounds with redox capabilities allows to increase the electrical charge stored in the system. Although this charge enhancement is not reflected in meaningful changes in the charge/mass ratio of the film, it does increase the charge/volume ratio and may be of great interest for the design of more compact charge storage devices. At this point it is important to consider that working with thin films allows a major part of the system to be accessible to the charge/discharge and ionic species exchange processes. The aim of the research reported in this manuscript is on the one hand the characterization of the material and to emphasize that it is precisely the in situ characterization techniques during the normal operation of the system (charge/discharge and ion exchange)[24,29,32,41] that will provide more precise information and therefore future optimization strategies for the operation of this kind of systems. To achieve these goals, several electrochemical coupled techniques were employed such as cyclic spectroelectrogravimetry with motional resistance measurement, digital video electrochemistry (DVEC) and ac-electrogravimetry [13–20].

2. EXPERIMENTAL

2.1. Generation

PEDOT deposition was performed by chronoamperometry using an AUTOLAB PGSTAB 302 applying 1.1 V during 14 s. The polymerization aqueous solution was 0.25 M KNO_3 (99%, Scharlau) and 0.01 M EDOT (97%, Sigma-Aldrich) with a pH of 5.4. All solutions were freshly prepared with distilled and deionized water (MilliQ-plus, Millipore, resistivity 18.2 MΩ cm). In all experiments, the auxiliary electrode was a Pt mesh, and the reference electrode was the Ag|AgCl|KCl$_{(sat)}$ electrode which all potentials are referred to (+0.197 V vs SHE at 298 K). As working electrodes, we used gold electrodes (electrode surface, S=0.2 cm^2) patterned on a 9 MHz quartz crystal resonator (TEMEX, France) or transparent indium tin oxide (ITO) electrodes (0.64 cm^2). Once PEDOT was deposited, cobalt ions were inserted into the film by voltammetry cycling between –0.6 V to 0.6 V at 10 mV s^{-1} using a 0.1 M $Co(NO_3)_2$ (99%, Scharlau) aqueous solution during 40 cycles to form PEDOT(Co) (pH=5.1). Finally, PEDOT(Co) was "activated" by repetitive voltammograms in 0.1M $LiClO_4$ (>95%, Sigma-Aldrich) aqueous solution at 10 mV s^{-1} between –0.6 V to 0.7 V to form PEDOT(aCo) (pH=7.0). To study the electroactivity of cobalt, nude EQCM gold electrodes were cycled by cyclic voltammetry between –0.6 V to 0.6 V at 10 mV s^{-1} in a 0.1 M $Co(NO_3)_2$ aqueous solution during 40 cycles (pH=5.1).

2.2. Characterization

PEDOT(aCo) was characterized by cyclic voltammetry at different scan rates, v, ranging from 10 mV s^{-1} to 200 mV s^{-1} between –0.6 to 0.7 V in 0.1 M $LiClO_4$ (pH=7.0). In the case of the experiment in de-airated atmosphere, the solution were previously deaerated by bubbling argon for 10 min before the experiment, keeping an atmosphere of argon during the experiment. The stability study of the system was carried out by cyclic voltammetry between –0.6 and 0.7 V at 200 mV s^{-1} for 100 cycles. A QCM-R (RQCM,

5

Maxtek Inc) microbalance and a Vis-NIR spectrometer (Maya 2000, Ocean optics) record gravimetric and spectroscopic responses during the voltammetric cycles. The electrochemical cell was a high- transmittance glass cell (Hellma, OG quality) with a 25×25 mm optical path length illuminated with a white LED strip (PowerLED, 6500 K) in a homemade white box. The X-ray energy dispersive Spectroscopy (EDX) analysis of the samples was performed using a Field Emission Scanning Electron Microscope (FE-SEM) Hitachi S4800, Tokyo, Japan (WD=15mm and HV=20kV).

The experimental Sauerbrey's constant to convert the QCM-R measurements into mass changes was $8.17\pm0.01\times10^8$ Hz g^{-1} cm^2. This was obtained from a galvanostatic deposition of copper by applying -8mA cm^{-2} during 150 s in a deaerated 0.5 M $CuSO_4$/0.1 M H_2SO_4 aqueous solution (pH 1.90) [62]. From electrogravimetry data, we can assess the species participating in the electrochemical reactions at a given potential calculating $F(dm/dQ)$ from dm/dt (in g s^{-1}) and current (in A) data as [24]:

$$F\frac{dm}{dQ} = \sum v_i \frac{M_i}{-z_i} \pm \xi \quad (1)$$

where F is the Faraday constant (96485 C mol^{-1}), ξ corresponds to the mass contribution of solvent or non-charged species. M_i is the molar mass of the i charged species involved in the faradaic process, z_i represents the electrical charge of the ion i that participates in the electrochemical process and v_i is the associated charge compensated by the participation of each i species. The sign of $F(dm/dQ)$ is prepared to indicate the species exchanged between the polymer and the electrolyte. In an ideal system considering only charged species, negative $F(dm/dQ)$ means that the electroactive system exchanges cations ($dm/dt<0$ and $dQ/dt>0$ or vice versa) whereas a positive $F(dm/dQ)$ indicates the exchange of anions ($dm/dt>0$ and $dQ/dt>0$ or vice versa). In real systems, the expected $F(dm/dQ)$ value for the charged participating species is subject to modification in some circumstances[22]:

i)   the simultaneous transfer of different species involving a combination of cations, anions and/or solvent. The non charged species as the solvent only involves mass change.

ii)   Capacitive currents or surface catalytic reactions that only consume charge without mass transfer. In the last case, $F(dm/dQ)$ tends to 0 g mol^{-1}.

iii)   Mathematically, $F(dm/dQ)$ tends to infinite when the current approaches to zero value. Around the potential where it takes place, $F(dm/dQ)$ loses its valuable analytical meaning.

2.3. Digital video electrochemistry

The color changes of PEDOT(aCo) deposited on ITO electrodes were characterized by DVEC using a commercial digital endoscope camera (Pontensic, B01059-P-NT) capturing 1280×720 pixels RGB digital videos at 30 frames per second. More information about the experimental set-up and other aspects of DVEC were explained in previous works [63,64].

6

Digital videos were recorded during the electrochemical characterizations and all frames were extracted. Cropped images of the area of interest for each of the frames were decomposed into three color arrays of RGB intensities by a home-made software. From a practical point of view due to a huge number of analyzed areas and pixels, the mean color intensities for each color array ($\bar{I}_R$, $\bar{I}_G$ and $\bar{I}_B$) were calculated as:

$$\bar{I} = \qquad (2)$$

where I_i is the color intensity of the pixel i and n_p is the total number of pixels in the analyzed area. For data interpretation, raw $\bar{I}$ data were appropriately smoothed using a Savitzky–Golay filter unless otherwise specified.

2.4. Electrochemical impedance spectroscopy and ac-electrogravimetry

Electrochemical Impedance Spectra (EIS) and ac-electrogravimetry (or Mass Impedance Spectroscopy) were obtained in 0.1 M LiClO$_4$ aqueous solution using a PAR 263A galvanostat-potentiostat, a SOLARTRON 1254A signal generator + frequency response analyzer and the frequency generator AGILENT 33220A. The microbalance was a lab-made oscillator built at UPR 15 CNRS Paris, France. All this equipment was controlled by home-made software. Set-up explained elsewhere [28,65,66]. Impedance data was recorded from 65 kHz to 10 mHz, with 5 points per decade with a potential perturbation amplitude of 25 mV *rms*. A home-made software based on the Marquardt least-squares procedure was used for the equivalent circuit fittings [67,68]. From EIS data, an analog function described in eq (1) can be obtained with the identical restrictions. The mixed transfer function $F\Delta m/\Delta q(\omega)$ is obtained from the ac-electrogravimetry transfer function, $\frac{\Delta m}{\Delta E}(\omega)$, and the capacitance one (eq (3)) as:

$$F\left(\frac{\Delta m}{\Delta q}\right)(\omega) = F\left(\frac{\frac{\Delta m}{\Delta E}(\omega)}{\frac{\Delta q}{\Delta E}(\omega)}\right) \qquad (3)$$

where ω is the angular frequency calculated from frequency perturbation (f) as $\omega = 2\pi f$

3.   RESULTS AND DISCUSSION

3.1. PEDOT generation

In all electrodes, EDOT was electropolymerized during 15 s in 0.01M EDOT and 0.25M KNO$_3$ aqueous solution by chronoamperometry while applying 1.1 V. Figure 1 shows current and mass evolution during the PEDOT electrodeposition on the gold surface. Once the monomers in solution underwent oxidation, the resulting radical cations reacts to generate polymer nuclei that precipitated onto the electrode surface. The current increased until reaching a maximum at 0.8 s. This process causes a rapid increase in mass due to the continuing polymerization of PEDOT on the electrode surface controlled by diffusion of monomer from the solution [69,70]. After this time, the mass exhibits a softer

positive slope which was due to the constant polymerization of PEDOT and simultaneous doping caused by film oxidation reaching about 12 μg cm^{-2} after the polymerization experiment and if we assume a film density of 1 g cm^{-3} [71] the thickness of PEDOT deposited is ~120 nm.

The inset of Figure 1 shows the $F\,dm/dq$ evolution during this process. After 5 seconds, the experimental value for this function is almost constant about +50-60 g mol^{-1}. Considering the mechanism proposed in [32]:

$$< Polymer > + EDOT + NO_3^- \rightarrow\, < Polymer - EDOT, NO_3^- > +2e^- \qquad (4)$$
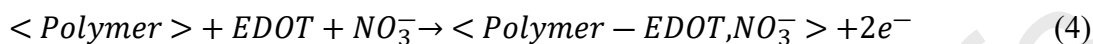
$F(dm/dq)$ should be close to +100 $g\,mol^{-1}$. One possible reason for this discrepancy is the exclusion of 2-3 water molecules inside the polymer by the nitrate doping. However, other factors as water oxidation or detachment of oligomers cannot be ignored. [72]. Finally, the PEDOT electrodeposition process in aqueous solution results in a blueish film doped with NO_3^-.

3.2. Cobalt insertion

Ion insertion in PEDOT depends on its oxidation state. PEDOT have shown p-doping process to compensate positive polarons and n-doping process to compensate negative polarons [73,74]. In addition, solvent transfer takes place simultaneously [41–43,75]. In a previous work, we detected lithium insertion during PEDOT reduction [32]. In this work, the oxidation state of PEDOT was repetitively changed by cyclic voltammetry between 0.6 V and –0.6 V at 10 mV s^{-1} in 0.1 M $Co(NO_3)_2$ aqueous solution (pH= 5.1)(Figure 2A).

During initial cycles, high cathodic currents are observed between –0.2V and –0.6V, which decrease with cycles. These cathodic currents are due a great reduction of PEDOT together with the catalyzed oxygen reduction [76]. The incorporation of cobalt ions (probably as Co^{2+}) occurs within this potential interval, where a significant increase in mass is observed (inset of Figure 2A). However, cobalt electrodeposition could be considered [77,78]. To elucidate this topic, we cycle a nude EQCM electrode in similar conditions (Figure 1SB in supplementary material). According to the work reported by E.M García et. al. [79], At pH>4.00 the electrodeposition of cobalt occurs via Co(OH)$_2$ intermediate with experimental values of 32 g mol^{-1} at –0.7 V at pH>4. As can be seen in Figure 1SA in supplementary material, there is an increase of the cathodic current intensity between –0.05V and –0.6V, with an increase of mass within the firsts 13 voltammetric cycles and smaller changes in the following ones. In the mentioned potential interval, the $F(dm/dQ)$ reaches –58 g mol^{-1} in the first cycles pointing to the participation of a single electron in the reduction process (Figure 1SB in supplementary material). This results suggests that a Co (I) species is adsorbed on the surface and quickly re-oxidized to Co^{2+} due to the instability of the species in aqueous media [80], forming Co(OH)$_2$ on the electrode surface since the formation of metallic cobalt is not consistent with $F(dm/dQ)$ results [79] and previous studies insomuch as Freitas et. al demonstrate that at pH 5.40 ionic cobalt (Co^{2+}) starts at -0.8V, before the reduction of H$^+$ and the mechanism of electrodeposition is a progressive nucleation that present a large nucleus size (three dimensional growth) [81].

In the range of potentials between −0.2V and −0.6V, $F(dm/dQ)$ reaches negatives values indicating cation insertion in all cycles (reduction direction of Figure 2S in supplementary materials). In the first cycle, $F(dm/dQ)$ is between −200 and −550 g mol^{-1}. If we assume the insertion of one cobalt (59 g mol^{-1}) per two electrons to keep the electroneutrality, between 10 and 30 water molecules are inserted simultaneously in the first scan. The insertion phenomenon of large atoms could open the PEDOT molecular structure allowing the entry of water by swelling [82]. In the successive cycles, $F(dm/dQ)$ show values about −[130, 60] g mol^{-1} indicating the entry of only 2-5 water molecules per cobalt insertion. Once PEDOT is hydrated, these values are reasonable taking into account the molar mass of hexaaquocolbat (173.07 g mol^{-1}) [42,75]. In the last cycle, $F(dm/dQ)$ is closer to 0 g mol^{-1} since the predominance of catalyzed oxygen reduction increases regarding the insertion of cobalt by the PEDOT reduction reaction (reduction direction of Figure 2S in in supplementary materials). In the oxidation direction, nitrate insertion with some water molecules is observed since $F(dm/dQ)$ values are higher that the molar mass of nitrate (oxidation direction of Figure 2S in in supplementary materials). In this occasion, water exclusion is not assumed as with other anions due to the small size of nitrates and the cobalt incorporation inside PEDOT which can lead to a more open structure facilitating the water insertion [41].

The increase of water molecules during cobalt insertion into PEDOT leads to the plasticization of PEDOT [75]. PEDOT stiffness is measured by the motional resistance (R_m) [20]. As shown in Figure 2B, R_m is maximum in the second voltammetric cycle, indicating a notable swelling of PEDOT due to the Co^{2+} incorporation with water molecules. This irreversible Co^{2+} incorporation increases the viscoelasticity of polymer since the structure of material is altered with a resonant frequency-motional resistance ratio ($\Delta f_r/\Delta R_m$) about 60 $Hz\,\Omega^{-1}$. The characteristic value of a net density/viscous effect is less than 10 $Hz\,\Omega^{-1}$ [20,83], therefore, we assume that PEDOT(Co) behaves as a acoustically rigid material. After this cycle, R_m decreases to stable value due to a moderate compaction of the generated PEDOT(Co) film.

As indicated by the mass evolution (Figure 2B), cobalt ions are irreversibly incorporated into PEDOT matrix as cycles progress during the initial 15 cycles in consonance with the mass and current variation on the bare Au electrode (see Figure 1S A (insert)). Thereafter, the film shows a saturation since the mass on the electrode remains almost constant about 58.4 $\mu g\,cm^{-2}$ (Figure 2B). Probably, the amount of cobalt incorporated into PEDOT to form the cobalt doped PEDOT (PEDOT(Co)) could be limited by the experimental conditions of PEDOT polymerization and cobalt insertion. Cobalt was homogeneously inserted in PEDOT as demonstrated by EDX analysis, (Figure 2C). Figure 3S in supplementary materials also indicates that nitrate ions are incorporated in the PEDOT structure which can supply fixed negative charges within the polymer.

3.3. PEDOT(Co) activation

After cobalt insertion, PEDOT(Co) system was cycled in 0.1M LiClO$_4$ aqueous solution. During first fifteen cycles, two additional pairs of current peaks emerge around 0.4 V, the oxidation peak corresponds to Co^{2+} to Co^{3+} reaction and the reduction peak at close potentials corresponds to Co^{3+} to Co^{2+} reaction, as if a new electrochemical process is activated due to the repetitive reduction and oxidation of PEDOT(Co) (Figure 3A). Simultaneously,

9

mass increases due to the irreversible insertion of the species from solution (Li^+, ClO_4^- and/or H_2O) (Figure 3B). The accommodation of species inside the polymer involves structural or conformational changes of the polymeric structure causing a moderate increase of viscoelasticity (Figure 3C) [75]. After this, stable parameters are achieved and we consider that PEDOT(Co) is fully electrochemically "activated" (PEDOT(aCo)). Figure 4A shows $F(dm/dQ)$ (eq (1)) for the second cycle of as representative result to discuss this "activation process" of PEDOT(Co). In this cycle, we assume perchlorate transfer since $F(dm/dQ)$ is higher than molar mass of nitrate (62 g mol⁻¹). Therefore, nitrates inside PEDOT are not exchanged (confirmed by EDX analysis in Figure 3S in supplementary materials). As occurs in PEDOT films, the anion transfer takes place at positive potentials, whereas, the cation transfer is placed in negative potentials [32].

First, we focus our discussion on the positive potentials window. From 0 V to 0.7 V, PEDOT(Co) oxidation involves the insertion of perchlorate ions with some extend of water exclusion since $F(dm/dQ)$ is around +65 g mol⁻¹, as observed in previous work[32]. During the reverse scan from 0.7V to –0.1V, the initial value of mass is not recovered (Figure 4B). Permanent insertion of perchlorate ions are discarded since no chlorine signals is detected in EDX analysis (Figure 3S in supplementary materials). Assuming the irreversible insertion of some water molecules, this process has a little effect on the viscoelastic properties of PEDOT(Co) since R_m is almost constant in this potential window (Figure 4C). Now, $F(dm/dQ)$ reaches values around +140 g mol⁻¹, which indicates the expulsion of anions accompanied with solvent molecules. At these potentials, PEDOT compaction is revealed by a gentle decrease of R_m.

In the negative potential interval, $F(dm/dQ)$ is about –65 g mol⁻¹ in the anodic and cathodic potential sweep (Figure 4A). In both sweeps, lithium ions with 2-3 water molecules are inserted, leading a significant increase in the mass (Figure 4B). This significant increase in mass is accumulated for the next cycle, as seen before, during 15 cycles. Therefore, we could assume the insertion of lithium and water inside the PEDOT in consonance with previous studies in bare PEDOT that indicate the lithium contribution such as counterion[32]. As a consequence, the viscoelasticity of system increases as revealed by R_m in Figure 4C (first from –0.1V to –0.6 and then, from –0.6V to 0V). After 15 cycles, the cyclic electrochemical, mass and R_m responses stabilize, indicating the complete activation of PEDOT(Co) to form the PEDOT(aCo). $\Delta f_r / \Delta R_m$ of the activation process is about 42 $Hz\ \Omega^{-1}$, therefore, PEDOT(aCo) keeps as a acoustically rigid film [20]. After the "activation" process, cobalt ions are irreversibly inserted into the hydrated PEDOT which stabilizes the new and altered electrochemistry of PEDOT (Figure 3S in supplementary materials) and nitrate irreversibly inserted.

3.4. Electrochemistry of PEDOT(aCo).

To understand the electrochemical nature of PEDOT(aCo), the voltammetry response of PEDOT and PEDOT(aCo) in similar conditions is compared. From Figure 5A, we can assume that the peaks system of PEDOT(aCo) around 0.4 V corresponds to the $Co^{2+} \rightleftarrows Co^{3+}$ in concordance with the literature [84] which enhances the capacity of storing charge regarding pristine PEDOT [32,41]. It is well-known that cobalt complexes provide lower positive potentials than aqua cobalt, or that metal-organic frameworks with sulfur stabilize cobalt ions [85–88]. Therefore, the electrochemistry of $Co^{2+} \rightleftarrows Co^{3+}$

reaction could be affected by the internal environment of PEDOT reducing its standard potential from 1.6 V to 0.4 V vs Ag|AgCl|KCl$_{sat}$.

The peak around −0.4V is due to the catalyzed reduction of dissolved oxygen in solution since the current intensity of the reduction peak in both PEDOT and PEDO(aCo) is less evident when voltammetry was repeated while bubbling argon into the electrolyte solution (Figure 5B). The voltammetry response of PEDOT(aCo) at different scan rates between 10-200 mV s^{-1} is presented in Figure 6A. Peak I ($Co^{2+} \rightarrow Co^{3+}$) and peak II ($Co^{3+} \rightarrow Co^{2+}$) together with the capacitive response of PEDOT at these potentials exhibit a linear relationship with the scan rate indicating a typical kinetic control of both processes (Figure 6B) [32]. Peak III varies linearly with the square root of scan rate verifying that the catalytic process of the oxygen reduction in aqueous media is under diffusional control (Figure 6C).

Figure 7 shows the dependence of $F(dm/dQ)$ with the scan rate for the peak I and peak III. At the peak I, we expect the insertion of anions during the oxidation of PEDOT. If only perchlorate ions are inserted, the theoretical value of $F(dm/dQ)$ is about +99 g mol^{-1}. However, $F(dm/dQ)$ is around +5 g mol^{-1} for all scan rates. On the one hand, the positive values indicate the insertion of perchlorate ions, but simultaneously the $Co^{2+} \rightarrow Co^{3+}$ reaction and the capacitive response of PEDOT(aCo) take place. Both processes involve an increase of charge but no mass changes. If, in addition, anions insertion into PEDOT films is accompanied by water expulsion (i.e. exclusion effect), low $F(dm/dQ)$ values as the observed are expected [41,42]. At fast scan rate, $F(dm/dQ)$ increases to +15 g mol^{-1}, therefore a second process could be overlapped. Around −0.4V (peak III), $F(dm/dQ)$ reaches values around −55 g mol^{-1} at 200 mV s^{-1}, indicating Li^+ insertion with some water molecules inside PEDOT(aCo) [32]. As the scan rate decreases, the catalytic current (a slow process compared to ion insertion) is more significant than the current due to reduction of PEDOT. For this reason, $F(dm/dQ)$ reduces to approximately −10 g mol^{-1} because the catalyzed oxygen reduction is a surface phenomenon which does not involve any mass changes.

The reversible color changes of PEDOT(aCo) during a voltammetry is first analyzed by digital video electrochemistry (DEVC) in the RGB color model. The fundamentals of this technique involve analyzing the alterations in color on the electrode surface through image analysis as explained elsewhere [89,90]. Figure 8 depicts the mean intensities of red, green, and blue colors (I_R, I_G, I_B) extracted from every pixel of the electroactive area of PEDOT(aCo) on ITO electrodes in a 0.1 M LiClO$_4$ aqueous solution. At approximately 0.5 V, we observe an RGB maximum (145,149,149) which coincides with the Co^{3+} accumulation inside PEDOT promoted by the $Co^{2+} \rightleftarrows Co^{3+}$ reaction evolution, leading to a light grey PEDOT(aCo). The reduced PEDOT(Co) is a grey-violet film with a (105,99,119) RGB coordinates at −0.7V. On the contrary, the pristine PEDOT is a darker film in both electrochemical forms (inset of Figure 8). These observations confirm the incorporation of cobalt ions into the PEDOT structure.

The spectroelectrochemical findings indicates that PEDOT(aCo) undergoes electrochromic changes between 500 and 1100 nm (Figure 9A). PEDOT exhibits spectroscopic changes between 400 and 750 nm associated with changes of thiophene ring [91,92]. Beyond 750 nm, the formation of polarons and bipolarons can be identified [91,93,94]. The reduced state of PEDOT(aCo) mainly absorbs between 400 and 900 nm,

11

whereas the oxidized state absorbs between 900 nm and 1100 nm (Figure 9B). At 925 nm, we observe a trend like in DVEC results (Figure 8), whereby PEDOT(aCo) oxidized at 0.5 V shows lesser absorption than a more oxidized state (0.7 V). Figure 9C-D shows dA^λ/dt at three selected wavelengths to determine the species formed during the voltammogram [32]. At 750 nm, positive polarons are detected during PEDOT(aCo) oxidation (dA^{750}/dt>0), and they disappear during the reduction (dA^{750}/dt<0), as showed in Figure 9C. The positive bipolarons are detected at 925 nm (Figure 9D) when the applied potential goes from −0.2 V to 0.4 V. However, the positive bipolarons disappear (dA^{925}/dt<0) and the amount of positive polarons increases again (peak of dA^{750}/dt at 0.5 V) at potentials where $Co^{2+} \rightarrow Co^{3+}$ starts. This evolution is not observed in pristine PEDOT [32]. During the PEDOT(Co) reduction from −0.2V to −0.6 V, the negative bipolarons in PEDOT(aCo) appear again. However, this kind of bipolarons is only observable at 1015 nm (Figure 9D), which suggest the formation of two structurally different types of bipolarons in the PEDOT(aCo) structure.

In the past two decades, the impedance techniques have emerged as a highly effective tool for investigating the electrochemical mechanisms in CPs. The combination of EIS and ac-electrogravimetry allows to discern between the role of anions and cations, as well as between fast and slow processes by the frequencies scan [95,28,29,96,97]. Figure 10 shows the impedance response in the capacitance mode (Cole-Cole diagram) of PEDOT(aCo) in 0.1 M LiClO$_4$ aqueous solution calculated from impedance ($Z(\omega)$) as:

$$C(\omega) = \frac{\Delta q}{\Delta E}(\omega) = \frac{1}{j\omega}(Z(\omega))^{-1} \quad (5)$$

where q is the charge, E is the potential, j is the imaginary number and ω is the angular frequency. Capacitance plot highlights the electrochemical response at low frequencies where CPs are actives.

At negative potentials, we observe one semicircle at higher frequencies due to the PEDOT(aCo) reduction and a branch at lower frequencies caused by the oxygen reduction (Figure 10). The equivalent circuit 1 characterize both processes as used for PEDOT films [32]. On the contrary, at positive potentials where the $Co^{2+} \rightleftarrows Co^{3+}$ reaction and PEDOT oxidation occur, PEDOT(aCo) shows one semicircle at high frequencies and a small branch at low frequencies. This behavior can be described by the equivalent circuit 2, as Figure 10 illustrates.

Table 1 lists the results of fitting the experimental data to the corresponding equivalent circuit. The uncompensated resistance ($R_u \approx$ 21 Ω) and the double layer capacitance ($C_{dl} \approx$ 0.5 mF) are minimally affected by the oxidation state of PEDOT(aCo). At all applied potentials, the electrochemical reactions of PEDOT have the fastest time constant (τ_p) calculated as:

$$\tau_p = R_p C_p \quad (6)$$

where R_p is the charge transfer resistance and C_p is the capacitance of the polymer. At negative potentials, the catalyzed reduction of oxygen is controlled by the diffusion of
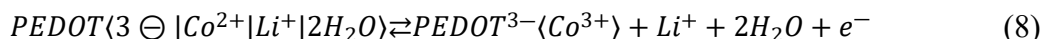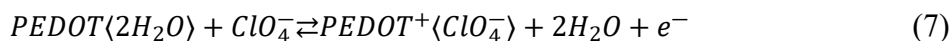
12

oxygen and is characterized by a resistance (R_O) and and Warburg element (W_O) [32]. At positive potentials, the slowest reaction is assigned to $Co^{2+} \rightleftarrows Co^{3+}$ characterized by the highest time constants (τ_{Co}) calculated from the charge transfer resistance (R_{Co}) and capacitance (C_{Co}) as in eq. (6). The sum of the capacitances of PEDOT and $Co^{2+} \rightleftarrows Co^{3+}$ reaction show that the cobalt incorporation increases about 46% of the charge store per amount of deposited PEDOT (about 85 $\mu F\ cm^2\ \mu g^{-1}$ at 0.56 V) regarding a pristine PEDOT in identical conditions (about 58 $\mu F\ cm^2\ \mu g^{-1}$ at 0.56 V) [32]. This enhancement could be profited by the manufacturing of charge storage devices.

Although EIS is an useful technique, it does not offer information about the nature of charged species transferred during the electrochemical processes [98]. To address this, ac-electrogravimetry has emerged as a powerful tool to discern among the role of cations, anions and solvent depending the position of semicircles on the complex plane plot [29,41,95–97]. In the analysis of ac-electrogravimetry results, we consider that the ionic and free solvent transfers at the polymer|solution interface are the rate-limiting steps since the species transports inside the film and in the solution are supposed to be fast enough for very thin films[99].

At potentials where PEDOT(aCo) is oxidized, the semicircles are positioned on the first quadrant indicating the main participation of anions, whereas the semicircles on the third quadrant at negative potentials indicate the main participation of cations [65,97,28]. The transition between quadrants is expected for two transfer processes with different time constants. At the higher frequencies and the positive potentials (Figure 11), PEDOT(aCo) shows a semicircle on the first quadrant, indicating that the fast insertion of anions compensates the oxidation of PEDOT [32]. At low frequencies, ac-electrogravimetry signal enters in the second quadrant where the relatively slower oxidation of inserted Co^{2+} increases the positive charges inside the system, leading the expulsion of cations. This fact may explain the increase in the storage of charge of PEDOT(aCo) regarding the PEDOT at these potentials (Figure 5). At negative potentials when PEDOT(aCo) is reduced, the semicircles on the third quadrant indicate the cation transfer to keep the electroneutrality of system [32]. At −0.1 V, we observe the transition between the oxidation and reduction processes.

By focusing our attention on the capacitive response of PEDOT(aCo) (at positive potentials), $F\Delta m/\Delta q(\omega)$ results (inset of Figure 11) allows us to suggest a possible doping-dedoping mechanism. At high frequencies, this function is approximately +50 g mol^{-1}. Assuming only PEDOT reactions (the faster process), the oxidation of PEDOT involves the insertion of one perchlorate ion ($M_w = 99$ g mol^{-1}) per transferred electron to compensate the formation of positive polarons (Figure 9C). This involves the simultaneous exclusion of 2-3 water molecules ($M_w = 18$ g mol^{-1}) [42]. At low frequencies, oxidation of inserted Co^{2+} (the slower process) occurs simultaneously with the PEDOT reactions and $F\Delta m/\Delta q(\omega)$ drops to about +10 g mol^{-1} since during $Co^{2+} \rightarrow Co^{3+}$ conversion, lithium ions ($M_w = 7$ g mol^{-1}) can be expulsed with 2-3 water molecules. This fact explains the slight increases of $F dm/dq$ observed at positive potentials in Figure 7. At the fastest scan rate, lithium transfer has more difficulties to takes place.

So, the proposed mechanism of PEDOT(aCo) at positive potentials could be summarized as:

$$PEDOT\langle 2H_2O\rangle + ClO_4^- \rightleftarrows PEDOT^+\langle ClO_4^-\rangle + 2H_2O + e^- \qquad (7)$$

$$PEDOT\langle 3 \ominus |Co^{2+}|Li^+|2H_2O\rangle \rightleftarrows PEDOT^{3-}\langle Co^{3+}\rangle + Li^+ + 2H_2O + e^- \qquad (8)$$

Here, we propose that three negative charges in PEDOT are fixed (negative bipolarons and/or nitrate ions) by one inner cobalt ion to keep the overall electroneutrality of system [73]. This assumption considers the formation of negative bipolarons only detected at 1015 nm (Figure 9D) and nitrogen and oxygen detection in EDX analysis (Figure 3S in supplementary materials). In addition, this could explain the irreversible insertion of cobalt ions inside PEDOT in consonance with previous works in similar systems [84] and the stability of Co^{2+} ion in aqueous medium at pH=7 and E > 0 V [80] (Figure 12). This was also observed in other conducting polymers where inner charges fixed by anions forces protons to be transferred to keep the electroneutrality [100]. On the contrary, cobalt should be exchanged as counterion in the re-oxidation of PEDOT.

Cyclic voltammetry was used to evaluate the electrochemical stability of the PEDOT(aCo) in 0.1M LiClO$_4$ aqueous solution, by applying a potential scan rate of 200mV s^{-1} between -0.6 and 0.7V. Figure 13A displays current response and demonstrate that PEDOT(Co) exhibits excellent cyclic stability after 100 cycles. Considering that the total mass deposited on the electrode during PEDOT(aCo) generation is about 70 μg cm^{-2} (about 12 μg cm^{-2} from PEDOT deposition and about 58 μg cm^{-2} from cobalt insertion), the mass loss after 100 cycles is only about 0.27% as shown in Figure 13B. In addition, PEDOT(aCo) viscoelastic properties remain stable during repetitive cycles, with a motional resistance value around 327 Ω (Figure 13C). These results are promising for the development of future charge storage devices.

4.   CONCLUSION.

The electrochemical performance of PEDOT(aCo) have been successfully investigated by coupled electrochemical techniques. Co^{2+} ions from a $Co(NO_3)_2$ aqueous solution have been irreversibly incorporated into PEDOT generated in aqueous media, apparently as $Co(OH)_2$. After activation in LiClO$_4$ aqueous solution, the resulting PEDOT(aCo) shows two new current peaks regarding pristine PEDOT at positive potentials The $Co^{2+} \rightleftarrows Co^{3+}$ conversion alters the colour transitions of PEDOT films with a different evolution of bipolaron formation than PEDOT. The incorporation of Co^{2+} involves slow transfer of cations for charge compensation during $Co^{2+} \rightleftarrows Co^{3+}$ conversion if we assume that the incorporated cobalt fix three negative charges inside PEDOT.While PEDOT electrochemistry keeps its faster processes by facilitating the transfer of anions to maintain electroneutrality. . The stable evolution of current, mass and viscoelasticity of PEDOT(aCo) suggests that this new material can be used in charge storage devices and more studies in terms of stability and feasibility should be carried out in future studies.

CRediT authorship contribution statement

Esteban Guillén: Investigation, Writing – original draft, Methodology, Data curation, Formal analysis. Jerónimo Agrisuelas, José J. García-Jareño, and Francisco Vicente:

Investigation, Validation, Formal analysis, Funding acquisition, Writing – review & editing.

Declaration of Competing Interest

The authors declare that they have no known competing financial interests or personal relationships that could influence the work reported in this paper.

ACKNOWLEDGMENTS

REFERENCES

[1] H. Zhang, V.V. Bhat, N.C. Gallego, C.I. Contescu, Thermal treatment effects on charge storage performance of graphene-based materials for supercapacitors, ACS Applied Materials & Interfaces 4 (2012) 3239–3246. https://doi.org/10.1021/am300593k.

[2] E. Hur, A. Arslan, Cobalt ion-doped polyaniline, poly(N-methylaniline), and poly(N-ethylaniline): electrosynthesis and characterisation using electrochemical methods in acidic solutions, Chem. Pap. 68 (2014) 1573–1583. https://doi.org/10.2478/s11696-014-0605-z.

[3] P. Sharma, V. Kumar, Current Technology of Supercapacitors: A Review, Journal of Electronic Materials 49 (2020) 3520–3532. https://doi.org/10.1007/s11664-020-07992-4.

[4] R. Gupta, A. Malik, K. Kumari, S.K. Singh, V. Vivier, P.C. Mondal, Metal-free platforms for molecular thin films as high-performance supercapacitors, Chem. Sci. (2024). https://doi.org/10.1039/d4sc00611a.

[5] J.R. Miller, P. Simon, Electrochemical Capacitors for Energy Management, Science 321 (2008) 651–652. https://doi.org/10.1126/science.1158736.

[6] J.R. Miller, A. Burke, Electrochemical Capacitors: Challenges and Opportunities for Real-World Applications, Electrochemical Society Interface 17 (2008) 53–57. https://doi.org/10.1201/9781420069709.ch8.

[7] V. Gupta, N. Miura, Polyaniline/single-wall carbon nanotube (PANI/SWCNT) composites for high performance supercapacitors, Electrochimica Acta 52 (2006) 1721–1726. https://doi.org/10.1016/j.electacta.2006.01.074.

[8]   K.V. Gurav, U.M. Patil, S.W. Shin, G.L. Agawane, M.P. Suryawanshi, S.M. Pawar, P.S. Patil, C.D. Lokhande, J.H. Kim, Room temperature chemical synthesis of Cu(OH)2 thin films for supercapacitor application, Journal of Alloys and Compounds 573 (2013) 27–31. https://doi.org/10.1016/j.jallcom.2013.03.193.

[9]   Z. Zhao, K. Xia, Y. Hou, Q. Zhang, Z. Ye, J. Lu, Designing flexible, smart and self-sustainable supercapacitors for portable/wearable electronics: from conductive polymers, Chem. Soc. Rev. 50 (2021) 12702–12743. https://doi.org/10.1039/D1CS00800E.

[10]   D. Mohanadas, Y. Sulaiman, Recent advances in development of electroactive composite materials for electrochromic and supercapacitor applications, Journal of Power Sources 523 (2022) 231029. https://doi.org/10.1016/j.jpowsour.2022.231029.

[11]   B. Gadgil, P. Damlin, E. Dmitrieva, T. Ääritalo, C. Kvarnström, ESR/UV-Vis-NIR spectroelectrochemical study and electrochromic contrast enhancement of a polythiophene derivative bearing a pendant viologen, RSC Advances 5 (2015) 42242–42249. https://doi.org/10.1039/C5RA04618A.

[12]   Z. Morávková, E. Dmitrieva, Structural changes in polyaniline near the middle oxidation peak studied by in situ Raman spectroelectrochemistry, J. Raman Spectrosc. 48 (2017) 1229–1234. https://doi.org/10.1002/jrs.5197.

[13]   A.R. Hillman, S. J. Daisley, S. Bruckenstein, Solvent effects on the electrochemical p-doping of PEDOT, Physical Chemistry Chemical Physics 9 (2007) 2379–2388. https://doi.org/10.1039/B618786B.

[14]   J. Agrisuelas, C. Gabrielli, J.J. García-Jareño, H. Perrot, F. Vicente, Kinetic and mechanistic aspects of a poly(o-toluidine)-modified gold electrode. 2. Alternating current electrogravimetry study in H2SO4 solutions, J. Phys. Chem. C 116 (2012) 15630–15640. https://doi.org/10.1021/jp303859m.

[15]   J. Arjomandi, Z. Kakaei, Electrosynthesis and In Situ Spectroelectrochemistry of Conducting o-aminophenol-p-aminophenol Copolymers in Aqueous Solution, J. Electrochem. Soc. 161 (2014) E53–E60. https://doi.org/10.1149/2.086403jes.

[16]   A. Malinauskas, R. Holze, A spectroelectrochemical study of the slow relaxation in polyaniline and its acceleration in composite films with poly(o-phenylenediamine), Phys. Chem. Chem. Phys. 101 (1997) 1851–1858.

[17]   M.J. Henderson, A.R. Hillman, E. Vieil, Ion and Solvent Transfer Discrimination at a Poly(o-toluidine) Film Exposed to HClO4 by Combined Electrochemical Quartz Crystal Microbalance (EQCM) and Probe Beam Deflection (PBD), J. Phys. Chem. B 103 (1999) 8899–8907. https://doi.org/10.1021/jp9910845.

[18]   G. Inzelt, Simultaneous chronoamperometric and quartz crystal microbalance studies of redox transformations of polyaniline films, Electrochim. Acta 45 (2000) 3865–3876. https://doi.org/10.1016/S0013-4686(00)00455-2.

[19]   J. Agrisuelas, J.J. García-Jareño, P. Rivas, J.M. Rodríguez-Mellado, F. Vicente, Electrochemistry and electrocatalysis of a Pt@poly(neutral red) hybrid

nanocomposite, Electrochim. Acta 171 (2015) 165–175. https://doi.org/10.1016/j.electacta.2015.04.120.

[20]   J. Agrisuelas, C. Gabrielli, J.J. García-Jareño, H. Perrot, O. Sel, F. Vicente, Viscoelastic potential-induced changes in acoustically thin films explored by quartz crystal microbalance with motional resistance monitoring, Electrochim. Acta 176 (2015) 1454–1463. https://doi.org/10.1016/j.electacta.2015.07.131.

[21]   Y. Zhang, B.D. Paulsen, E.A. Schafer, Q. Zeng, F. Yu, L. Yang, Y. Xue, J. Rivnay, N. Zhao, Combined Optical, Gravimetric, and Electrical Operando Investigation of Structural Variations in Polymeric Mixed Conductors, Advanced Functional Materials 33 (2023) 2214380. https://doi.org/10.1002/adfm.202214380.

[22]   J.J. García-Jareño, J. Agrisuelas, F. Vicente, Overview and Recent Advances in Hyphenated Electrochemical Techniques for the Characterization of Electroactive Materials, Materials 16 (2023) 4226. https://doi.org/10.3390/ma16124226.

[23]   J. Agrisuelas, C. Gabrielli, J.J. García-Jareño, H. Perrot, F. Vicente, Kinetic and mechanistic aspects of a poly(o-toluidine)-modified gold electrode. 1. Simultaneous cyclic spectroelectrochemistry and electrogravimetry studies in H2SO4 solutions, J. Phys. Chem. C 116 (2012) 15620–15629. https://doi.org/10.1021/jp303858q.

[24]   J. Agrisuelas, C. Gabrielli, J.J. Garcia-Jareno, D. Gimenez-Romero, J. Gregori, H. Perrot, F. Vicente, Usefulness of F(dm/dQ) function for elucidating the ions role in PB films, J. Electrochem. Soc. 154 (2007) F134–F140. https://doi.org/10.1149/1.2728038.

[25]   J. Agrisuelas, D. Giménez-Romero, J.J. García-Jareño, F. Vicente, Vis/NIR spectroelectrochemical analysis of poly-(Azure A) on ITO electrode, Electrochem. Commun. 8 (2006) 549–553. https://doi.org/10.1016/j.elecom.2006.01.022.

[26]   D. Giménez-Romero, P.R. Bueno, C. Gabrielli, C. Castaño, H. Perrot, J.J. García-Jareño, F. Vicente, Mass/charge balance as a tool to estimate dimensional change in polypyrrole-based actuators, Electrochem. Commun. 8 (2006) 195–199. https://doi.org/10.1016/j.elecom.2005.11.007.

[27]   T. Amemiya, K. Hashimoto, A. Fujishima, COLOR IMPEDANCE SPECTROSCOPY OF POLYPYRROLE FILMS, Journal of Electroanalytical Chemistry 377 (1994) 143–148.

[28]   J. Agrisuelas, J.J. García-Jareño, D. Gimenez-Romero, F. Vicente, Innovative combination of three alternating current relaxation techniques: electrical charge, mass, and color impedance spectroscopy. Part I: the tool, J. Phys. Chem. C 113 (2009) 8430–8437. https://doi.org/10.1021/jp900823z.

[29]   J. Agrisuelas, J.J. García-Jareño, D. Gimenez-Romero, F. Vicente, Innovative combination of three alternating current relaxation techniques: electrical charge, mass, and color impedance spectroscopy. Part II: prussian blue ⇄ Everitt's salt process, J. Phys. Chem. C 113 (2009) 8438–8446. https://doi.org/10.1021/jp900824w.

[30]   R.J. da Silva, R.M.A.P. Lima, M.C.A. de Oliveira, J.J. Alcaraz-Espinoza, C.P. de Melo, H.P. de Oliveira, Supercapacitors based on (carbon nanostructure)/PEDOT/(eggshell membrane) electrodes, Journal of Electroanalytical Chemistry 856 (2020) 113658. https://doi.org/10.1016/j.jelechem.2019.113658.

[31]   Y. Han, Enhanced electrical properties of PEDOT:PSS via synergistic effect, Soft Materials 16 (2018) 31–36. https://doi.org/10.1080/1539445X.2017.1387151.

[32]   E. Guillén, J. Agrisuelas, J.J. García-Jareño, F. Vicente, The role of lithium, perchlorate and water during electrochemical processes in poly(3,4-ethylenedioxythiophene) films in LiClO4 aqueous solutions, Journal of Electroanalytical Chemistry 897 (2021) 115580. https://doi.org/10.1016/j.jelechem.2021.115580.

[33]   H.A. Khan, M. Tawalbeh, B. Aljawrneh, W. Abuwatfa, A. Al-Othman, H. Sadeghifar, A.G. Olabi, A comprehensive review on supercapacitors: Their promise to flexibility, high temperature, materials, design, and challenges, Energy 295 (2024) 131043. https://doi.org/10.1016/j.energy.2024.131043.

[34]   Yu.M. Volfkovich, High power supercapacitors. Review, Journal of Electroanalytical Chemistry 963 (2024) 118290. https://doi.org/10.1016/j.jelechem.2024.118290.

[35]   Y. Fan, T. Wang, R. Asrosa, B. Li, N. Naresh, X. Liu, S. Guan, R. Li, M. Wang, I.P. Parkin, B.D. Boruah, Synergistic contribution of activated carbon and PEDOT:PSS in hybrid electrodes for high-performance planar micro-supercapacitors, Chemical Engineering Journal 488 (2024) 150672. https://doi.org/10.1016/j.cej.2024.150672.

[36]   X. Wang, A. Abdurexit, R. Jamal, T. Abdiryim, N. Fan, Y. Liu, K. Song, H. Yang, Preparation of PEDOT/Ti3C2Tx/Co3S2 composite for quasi−solid−state hybrid supercapacitor with enhanced electrochemical performance, Journal of Alloys and Compounds 980 (2024) 173609. https://doi.org/10.1016/j.jallcom.2024.173609.

[37]   L. Groenendaal, F. Jonas, D. Freitag, H. Pielartzik, J.R. Reynolds, Poly(3,4-ethylenedioxythiophene) and Its Derivatives: Past, Present, and Future, Advanced Materials 12 (2000) 481–494. https://doi.org/10.1002/(SICI)1521-4095(200004)12:7<481::AID-ADMA481>3.0.CO;2-C.

[38]   S. Kirchmeyer, K. Reuter, Scientific importance, properties and growing applications of poly(3,4-ethylenedioxythiophene), J. Mater. Chem. 15 (2005) 2077–2088. https://doi.org/10.1039/B417803N.

[39]   C. Arbizzani, M. Mastragostino, F. Soavi, New trends in electrochemical supercapacitors, J. Power Sources 100 (2001) 164–170. https://doi.org/10.1016/S0378-7753(01)00892-8.

[40]   A.R. Hillman, S.J. Daisley, S. Bruckenstein, Kinetics and mechanism of the electrochemical p-doping of PEDOT, Electrochemistry Communications 9 (2007) 1316–1322. https://doi.org/10.1016/j.elecom.2007.01.009.

[41]   J. Agrisuelas, C. Gabrielli, J.J. García-Jareño, H. Perrot, O. Sel, F. Vicente, Electrochemically induced free solvent transfer in thin poly(3,4-ethylenedioxythiophene) films, Electrochim. Acta 164 (2015) 21–30. https://doi.org/10.1016/j.electacta.2015.02.133.

[42]   A. Bund, S. Neudeck, Effect of the Solvent and the Anion on the Doping/Dedoping Behavior of Poly(3,4-ethylenedioxythiophene) Films Studied with the Electrochemical Quartz Microbalance, J. Phys. Chem. B 108 (2004) 17845–17850. https://doi.org/10.1021/jp0469721.

[43]   W. Plieth, A. Bund, U. Rammelt, S. Neudeck, L. Duc, The role of ion and solvent transport during the redox process of conducting polymers, Electrochimica Acta 51 (2006) 2366–2372. https://doi.org/10.1016/j.electacta.2005.03.087.

[44]   T. Le, D. Aradilla, G. Bidan, F. Billon, C. Debiemme-Chouvy, H. Perrot, O. Sel, Charge Storage Properties of Nanostructured Poly (3,4-ethylenedioxythiophene) Electrodes Revealed by Advanced Electrogravimetry, Nanomaterials 9 (2019) 962. https://doi.org/10.3390/nano9070962.

[45]   Z.-Q. Feng, J. Wu, W. Cho, M.K. Leach, E.W. Franz, Y.I. Naim, Z.-Z. Gu, J.M. Corey, D.C. Martin, Highly aligned poly(3,4-ethylene dioxythiophene) (PEDOT) nano- and microscale fibers and tubes, Polymer 54 (2013) 702–708. https://doi.org/10.1016/j.polymer.2012.10.057.

[46]   C. Yuan, L. Yang, L. Hou, J. Li, Y. Sun, X. Zhang, L. Shen, X. Lu, S. Xiong, X.W. Lou, Flexible hybrid paper made of monolayer Co 3O 4 microsphere arrays on rGO/CNTs and their application in electrochemical capacitors, Advanced Functional Materials 22 (2012) 2560–2566. https://doi.org/10.1002/adfm.201102860.

[47]   H.-J. Kim, S.Y. Kim, L.J. Lim, A.E. Reddy, C.V.V.M. Gopi, Facile one-step synthesis of a composite CuO/Co3O4 electrode material on Ni foam for flexible supercapacitor applications, New Journal of Chemistry 41 (2017) 5493–5497. https://doi.org/10.1039/c7nj01109a.

[48]   J. Hao, S. Peng, H. Li, S. Dang, T. Qin, Y. Wen, J. Huang, F. Ma, D. Gao, F. Li, G. Cao, A low crystallinity oxygen-vacancy-rich Co3O4 cathode for high-performance flexible asymmetric supercapacitors, Journal of Materials Chemistry A 6 (2018) 16094–16100. https://doi.org/10.1039/c8ta06349d.

[49]   E. Duraisamy, H.T. Das, A. Selva Sharma, P. Elumalai, Supercapacitor and photocatalytic performances of hydrothermally-derived Co3O4/CoO@carbon nanocomposite, New Journal of Chemistry 42 (2018) 6114–6124. https://doi.org/10.1039/c7nj04638c.

[50]   K.T. Nam, D.-W. Kim, P.J. Yoo, C.-Y. Chiang, N. Meethong, P.T. Hammond, Y.-M. Chiang, A.M. Belcher, Virus-enabled synthesis and assembly of nanowires for lithium ion battery electrodes, Science 312 (2006) 885–888. https://doi.org/10.1126/science.1122716.

[51]   H.-K. Kim, T.-Y. Seong, J.-H. Lim, W. Ii Cho, Y. Soo Yoon, Electrochemical and structural properties of radio frequency sputtered cobalt oxide electrodes for thin-film

supercapacitors, Journal of Power Sources 102 (2001) 167–171. https://doi.org/10.1016/S0378-7753(01)00864-3.

[52] Z.-S. Wu, W. Ren, L. Wen, L. Gao, J. Zhao, Z. Chen, G. Zhou, F. Li, H.-M. Cheng, Graphene anchored with Co3O4 nanoparticles as anode of lithium ion batteries with enhanced reversible capacity and cyclic performance, ACS Nano 4 (2010) 3187–3194. https://doi.org/10.1021/nn100740x.

[53] X. Wang, X.-L. Wu, Y.-G. Guo, Y. Zhong, X. Cao, Y. Ma, J. Yao, Synthesis and lithium storage properties of Co3O4 nanosheet-assembled multishelled hollow spheres, Advanced Functional Materials 20 (2010) 1680–1686. https://doi.org/10.1002/adfm.200902295.

[54] S. Xiong, C. Yuan, X. Zhang, B. Xi, Y. Qian, Controllable Synthesis of Mesoporous Co3O4 Nanostructures with Tunable Morphology for Application in Supercapacitors, Chemistry – A European Journal 15 (2009) 5320–5326. https://doi.org/10.1002/chem.200802671.

[55] Y. Sulaiman, M.K.S. Azmi, M.A.A. Mohd Abdah, N.H.N. Azman, One step electrodeposition of poly-(3,4-ethylenedioxythiophene)/graphene oxide/cobalt oxide ternary nanocomposite for high performance supercapacitor, Electrochimica Acta 253 (2017) 581–588. https://doi.org/10.1016/j.electacta.2017.09.103.

[56] P.T. Lim, N.H.N. Azman, S. Kulandaivalu, Y. Sulaiman, Three-dimensional network of poly(3,4-ethylenedioxythiophene)/nanocrystalline cellulose/cobalt oxide for supercapacitor, Polymer 250 (2022) 124888. https://doi.org/10.1016/j.polymer.2022.124888.

[57] N.H. Nabilah Azman, Y. Sulaiman, Supercapattery performance of carbon nanofibers decorated with poly(3,4-ethlenedioxythiophene) and cobalt oxide, Ceramics International 48 (2022) 11772–11778. https://doi.org/10.1016/j.ceramint.2022.01.036.

[58] D.D. Mohite, S.S. Chavan, P.E. Lokhande, K.B. Sutar, S. Dubal, U. Rednam, B. Ali Al-Asbahi, Y. Anil Kumar, Metal oxide-based nanocomposites as advanced electrode materials for enhancing electrochemical performance of Supercapacitors: A comprehensive review, Materials Today: Proceedings (2024). https://doi.org/10.1016/j.matpr.2024.05.001.

[59] N.S. George, L.M. Jose, A. Aravind, N.S. George, L.M. Jose, A. Aravind, Review on Transition Metal Oxides and Their Composites for Energy Storage Application, in: Updates on Supercapacitors, IntechOpen, 2022. https://doi.org/10.5772/intechopen.108781.

[60] J. Iqbal, A. Numan, S. Rafique, R. Jafer, S. Mohamad, K. Ramesh, S. Ramesh, High performance supercapattery incorporating ternary nanocomposite of multiwalled carbon nanotubes decorated with Co3O4 nanograins and silver nanoparticles as electrode material, Electrochimica Acta 278 (2018) 72–82. https://doi.org/10.1016/j.electacta.2018.05.040.

[61] E. Hür, A. Arslan, New electrode active materials for supercapacitors: Pencil graphite electrode coated with cobalt ion doped poly(3-methylthiophene) and

poly(3,4-ethylenedioxythiophene), Synthetic Metals 193 (2014) 81–88. https://doi.org/10.1016/j.synthmet.2014.03.031.

[62]   A. Cuenca, J. Agrisuelas, J.J. García-Jareño, F. Vicente, Oscillatory Changes of the Heterogeneous Reactive Layer Detected with the Motional Resistance during the Galvanostatic Deposition of Copper in Sulfuric Solution, Langmuir 31 (2015) 12664–12673. https://doi.org/10.1021/acs.langmuir.5b03694.

[63]   J. Agrisuelas, J.J. García-Jareño, E. Perianes, F. Vicente, Use of RGB digital video analysis to study electrochemical processes involving color changes, Electrochem. Commun. 78 (2017) 38–42. https://doi.org/10.1016/j.elecom.2017.04.001.

[64]   J. Agrisuelas, J.J. García-Jareño, F. Vicente, Spatiotemporal colorimetry to reveal electrochemical kinetics of poly(o-toluidine) films along ITO surface, Electrochim. Acta 269 (2018) 350–358. https://doi.org/10.1016/j.electacta.2018.02.157.

[65]   J.J. García-Jareño, D. Giménez-Romero, F. Vicente, C. Gabrielli, M. Keddam, H. Perrot, EIS and Ac-Electrogravimetry Study of PB Films in KCl, NaCl, and CsCl Aqueous Solutions, J. Phys. Chem. B 107 (2003) 11321–11330. https://doi.org/10.1021/jp035387h.

[66]   C. Gabrielli, J.J. García-Jareño, M. Keddam, H. Perrot, F. Vicente, Ac-Electrogravimetry Study of Electroactive Thin Films. I. Application to Prussian Blue, J. Phys. Chem. B 106 (2002) 3182–3191. https://doi.org/10.1021/jp013924x.

[67]   J.R. Macdonald, Impedance spectroscopy: Models, data fitting, and analysis, Solid State Ionics 176 (2005) 1961–1969. https://doi.org/10.1016/j.ssi.2004.05.035.

[68]   J.J. García-Jareño, J.J. Navarro, A.F. Roig, H. Scholl, F. Vicente, Impedance analysis of Prussian Blue films deposited on ITO electrodes, Electrochimica Acta 40 (1995) 1113–1119. https://doi.org/10.1016/0013-4686(95)00017-9.

[69]   L. Pigani, A. Heras, Á. Colina, R. Seeber, J. López-Palacios, Electropolymerisation of 3,4-ethylenedioxythiophene in aqueous solutions, Electrochemistry Communications 6 (2004) 1192–1198. https://doi.org/10.1016/j.elecom.2004.09.021.

[70]   M.J. González-Tejera, I. Carrillo Ramiro, I. Hernández-Fuentes, Nucleation and growth mechanism of polyfurane perchlorate doped films, Electrochimica Acta 45 (2000) 1973–1982. https://doi.org/10.1016/S0013-4686(99)00416-8.

[71]   J. Bobacka, A. Lewenstam, A. Ivaska, Electrochemical impedance spectroscopy of oxidized poly(3,4-ethylenedioxythiophene) film electrodes in aqueous solutions, Journal of Electroanalytical Chemistry 489 (2000) 17–27. https://doi.org/10.1016/S0022-0728(00)00206-0.

[72]   E. Ventosa, A. Colina, A. Heras, A. Martínez, O. Orcajo, V. Ruiz, J. López-Palacios, Electrochemical, spectroscopic and electrogravimetric detection of oligomers occluded in electrochemically synthesized poly(3,4-ethylenedioxythiophene) films, Electrochimica Acta 53 (2008) 4219–4227. https://doi.org/10.1016/j.electacta.2007.12.064.

[73] H.J. Ahonen, J. Lukkari, J. Kankare, n- and p-Doped Poly(3,4-ethylenedioxythiophene): Two Electronically Conducting States of the Polymer, Macromolecules 33 (2000) 6787–6793. https://doi.org/10.1021/ma0004312.

[74] P.S. Tóth, C. Janáky, O. Berkesi, T. Tamm, C. Visy, On the Unexpected Cation Exchange Behavior, Caused by Covalent Bond Formation between PEDOT and Cl– Ions: Extending the Conception for the Polymer–Dopant Interactions, J. Phys. Chem. B 116 (2012) 5491–5500. https://doi.org/10.1021/jp2107268.

[75] V. Lyutov, V. Gruia, I. Efimov, A. Bund, V. Tsakova, An acoustic impedance study of PEDOT layers obtained in aqueous solution, Electrochimica Acta 190 (2016) 285–293. https://doi.org/10.1016/j.electacta.2015.12.177.

[76] F. Sarrami, V. Gueskine, I. Zozoulenko, Electrochemical oxygen reduction reaction at conductive polymer PEDOT: Insight from ab initio molecular dynamics simulations, Chemical Physics 551 (2021) 111308. https://doi.org/10.1016/j.chemphys.2021.111308.

[77] L.H. Mendoza-Huizar, J. Robles, M. Palomar-Pardavé, Nucleation and growth of cobalt onto different substrates: Part I. Underpotential deposition onto a gold electrode, Journal of Electroanalytical Chemistry 521 (2002) 95–106. https://doi.org/10.1016/S0022-0728(02)00659-9.

[78] K. Kim, D. Raymond, R. Candeago, X. Su, Selective cobalt and nickel electrodeposition for lithium-ion battery recycling through integrated electrolyte and interface control, Nat Commun 12 (2021) 6554. https://doi.org/10.1038/s41467-021-26814-7.

[79] E.M. Garcia, J.S. Santos, E.C. Pereira, M.B.J.G. Freitas, Electrodeposition of cobalt from spent Li-ion battery cathodes by the electrochemistry quartz crystal microbalance technique, Journal of Power Sources 185 (2008) 549–553. https://doi.org/10.1016/j.jpowsour.2008.07.011.

[80] J. Chivot, L. Mendoza, C. Mansour, T. Pauporté, M. Cassir, New insight in the behaviour of Co–H2O system at 25–150°C, based on revised Pourbaix diagrams, Corrosion Science 50 (2008) 62–69. https://doi.org/10.1016/j.corsci.2007.07.002.

[81] M.B.J.G. Freitas, E.M. Garcia, Electrochemical recycling of cobalt from cathodes of spent lithium-ion batteries, Journal of Power Sources 171 (2007) 953–959. https://doi.org/10.1016/j.jpowsour.2007.07.002.

[82] J.L. Antonio, L. Höfler, T. Lindfors, S.I. Córdoba de Torresi, Electrocontrolled Swelling and Water Uptake of a Three-Dimensional Conducting Polypyrrole Hydrogel, ChemElectroChem 3 (2016) 2146–2152. https://doi.org/10.1002/celc.201600397.

[83] S.J. Martin, V.Edwards. Granstaff, G.C. Frye, Characterization of a quartz crystal microbalance with simultaneous mass and liquid loading, Anal. Chem. 63 (1991) 2272–2281. https://doi.org/10.1021/ac00020a015.

[84] R.P. Kingsborough, T.M. Swager, Electroactivity Enhancement by Redox Matching in Cobalt Salen–Based Conducting Polymers, Advanced Materials 10

(1998) 1100–1104. https://doi.org/10.1002/(SICI)1521-4095(199810)10:14<1100::AID-ADMA1100>3.0.CO;2-2.

[85] P. Buglyó, I. Kacsir, M. Kozsup, I. Nagy, S. Nagy, A.C. Bényei, É. Kováts, E. Farkas, Tuning the redox potentials of ternary cobalt(III) complexes containing various hydroxamates, Inorganica Chimica Acta 472 (2018) 234–242. https://doi.org/10.1016/j.ica.2017.07.026.

[86] C.V. Garcia, G.L. Parrilha, B.L. Rodrigues, P.J.S. Barbeira, R.M. Clarke, T. Storr, H. Beraldo, Cobalt(III) complexes with 2-acetylpyridine-derived Schiff bases: Studies investigating ligand release upon reduction, Polyhedron 124 (2017) 86–95. https://doi.org/10.1016/j.poly.2016.12.024.

[87] R.-Y. Fan, J.-Y. Xie, Y. Ma, J.-Y. Fu, H.-J. Liu, M.-X. Li, W.-L. Yu, D.-P. Liu, Y.-M. Chai, B. Dong, Structure optimization and electronic modulation of sulfur-incorporated cobalt nanocages for enhanced oxygen evolution, International Journal of Hydrogen Energy 46 (2021) 28537–28544. https://doi.org/10.1016/j.ijhydene.2021.06.080.

[88] F. Yu, H. Zhou, Q. Shen, Modification of cobalt-containing MOF-derived mesoporous carbon as an effective sulfur-loading host for rechargeable lithium-sulfur batteries, Journal of Alloys and Compounds 772 (2019) 843–851. https://doi.org/10.1016/j.jallcom.2018.09.103.

[89] E. Guillén, J. Agrisuelas, J.J. García-Jareño, F. Vicente, Electrochromic Performances of Poly(Azure A) Films from Digital Video-Electrochemistry (DVEC), J. Electrochem. Soc. 167 (2020) 106514. https://doi.org/10.1149/1945-7111/ab9e3b.

[90] E. Guillén, M. Ferrer-Roselló, J. Agrisuelas, J.J. García-Jareño, F. Vicente, Digital video-electrochemistry (DVEC) to assess electrochromic materials in the frequency domain: RGB colorimetry impedance spectroscopy, Electrochimica Acta 366 (2021) 137340. https://doi.org/10.1016/j.electacta.2020.137340.

[91] S. Duluard, B. Ouvrard, A. Celik-Cochet, G. Campet, U. Posset, G. Schottner, M.-H. Delville, Comparison of PEDOT Films Obtained via Three Different Routes through Spectroelectrochemistry and the Differential Cyclic Voltabsorptometry Method (DCVA), J. Phys. Chem. B 114 (2010) 7445–7451. https://doi.org/10.1021/jp9111712.

[92] L. Beverina, G.A. Pagani, M. Sassi, Multichromophoric electrochromic polymers: colour tuning of conjugated polymers through the side chain functionalization approach, Chem. Commun. 50 (2014) 5413–5430. https://doi.org/10.1039/C4CC00163J.

[93] T. Kim, J. Kim, Y. Kim, T. Lee, W. Kim, K.S. Suh, Preparation and characterization of poly(3,4-ethylenedioxythiophene) (PEDOT) using partially sulfonated poly(styrene-butadiene-styrene) triblock copolymer as a polyelectrolyte, Current Applied Physics 9 (2009) 120–125. https://doi.org/10.1016/j.cap.2007.12.005.

[94]   D. Hohnholz, A.G. MacDiarmid, D.M. Sarno, W.E. Jones, Uniform thin films of poly-3,4-ethylenedioxythiophene (PEDOT) prepared by in-situ deposition, Chem. Commun. (Camb.) (2001) 2444–2445.

[95]   C. Gabrielli, M. Keddam, N. Nadi, H. Perrot, ac Electrogravimetry on conducting polymers. Application to polyaniline, in: Workshop on the Electrochemistry of Electroactive Polymer FILMS (WEEPF97), Dourdan, France, 1997: pp. 2095–2103.

[96]   C. Gabrielli, M. Keddam, N. Nadi, H. Perrot, Ions and solvent transport across conducting polymers investigated by ac electrogravimetry. Application to polyaniline, J. Electroanal. Chem. 485 (2000) 101–113. https://doi.org/10.1016/S0022-0728(00)00093-0.

[97]   C. Gabrielli, J.J. Garcia-Jareno, M. Keddam, H. Perrot, F. Vicente, Ac-Electrogravimetry Study of Electroactive Thin Films. I. Application to Prussian Blue, The Journal of Physical Chemistry B 106 (2002) 3182–3191. https://doi.org/10.1021/jp013924x.

[98]   J. Pedro Aguiar dos Santos, F. Cesar Rufino, J.I. Yutaka Ota, R.C. Fernandes, R. Vicentini, C.J.B. Pagan, L. Morais Da Silva, H. Zanin, Best practices for electrochemical characterization of supercapacitors, Journal of Energy Chemistry 80 (2023) 265–283. https://doi.org/10.1016/j.jechem.2022.12.034.

[99]   C. Gabrielli, H. Perrot, AC-Electrogravimetry Investigation in Electroactive Thin Films, in: M. Schlesinger (Ed.), Modern Aspects of Electrochemistry No. 44: Modelling and Numerical Simulations II, Springer, New York, NY, 2009: pp. 151–238. https://doi.org/10.1007/978-0-387-49586-6_5.

[100] E. Guillén, A. Ferrer, J. Agrisuelas, J.J. García-Jareño, F. Vicente, Spectroelectrogravimetry of the electrical conductivity activation in poly(o-toluidine) films, J Solid State Electrochem 24 (2020) 2353–2363. https://doi.org/10.1007/s10008-020-04754-4.

TABLES

Table 1. Impedance measurements from the fittings of impedance data with the equivalent circuits in Figure 10.

E/V	R_u/Ω	C_{dl}/μF	R_p/Ω	C_p/mF	τ_p/ms	R_O/kΩ	W_O/ kΩ s$^{-}_{0.5}$
−0.10	20	4.5	1.2	0.53	0.6	23	2.3
−0.38	20	4.5	0.7	0.51	0.4	9	1.25
−0.50	20	4.5	1.0	0.47	0.5	12	5.2

E/V	R_u/Ω	C_{dl}/μF	R_p/Ω	C_p/mF	τ_p/ms	R_{Co}/kΩ	C_{Co}/mF	τ_{Co}/s
0.22	20	4.5	1.3	0.46	0.6	35	0.13	4.53
0.32	20	4.5	0.7	0.49	0.4	27	0.32	8.7
0.56*	20	4.5	0.0	0.82	-	176	-	-

*This potential correspond to the Co^{2+}/Co^{3+} process. The equivalent circuit is $R_u+(C_{dl}\#(R_p+C_p)\#R_{Co})$. "+" indicate component in serie, and "#" in parallel.

FIGURES
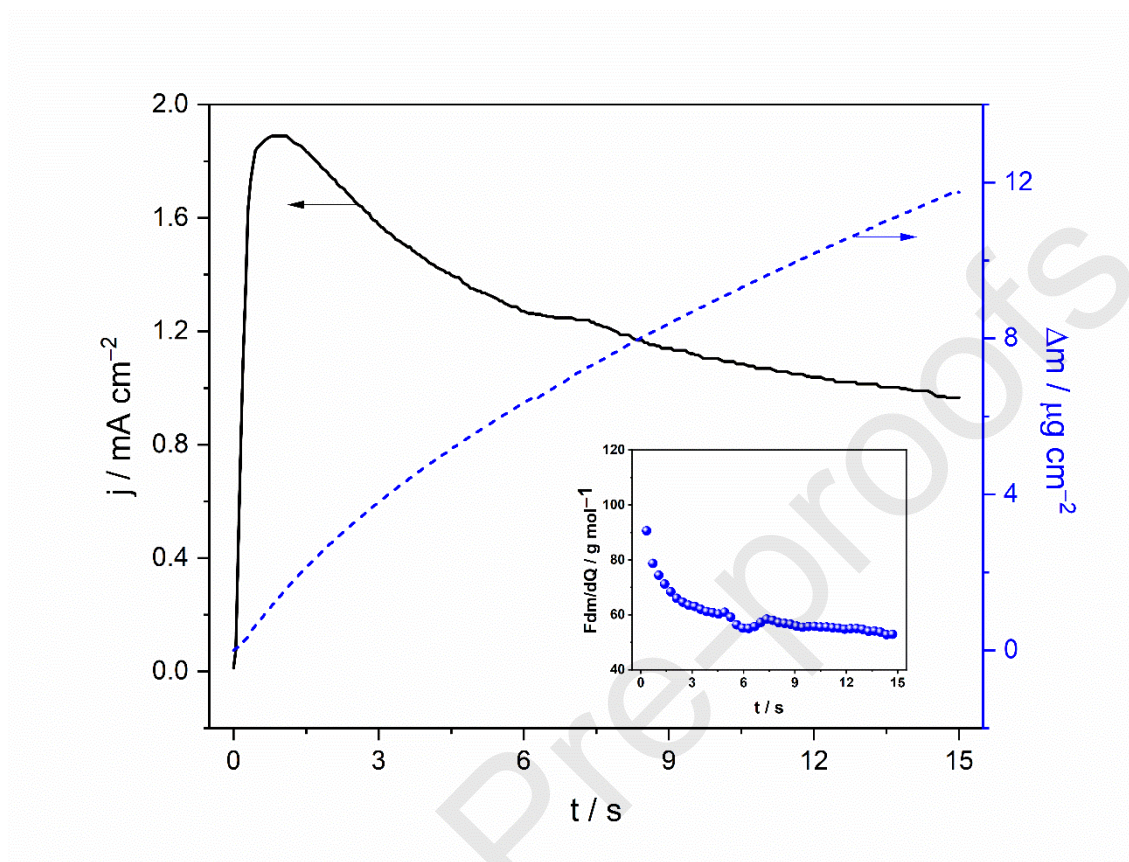
Figure 1. PEDOT polymerization on EQCM electrode by chronoamperometry during 15 s in 0.01 M EDOT, 0.25 M KNO$_3$ aqueous solution applying 1.1 V (pH=5.4). The inset shows the $F(dm/dq)$ (eq. (1)) during the polymerization process. The auxiliary electrode was a Pt mesh, and the reference electrode was the Ag|AgCl|KCl$_{(sat)}$ electrode which all potentials are referred to (+0.197 V vs SHE at 298 K).
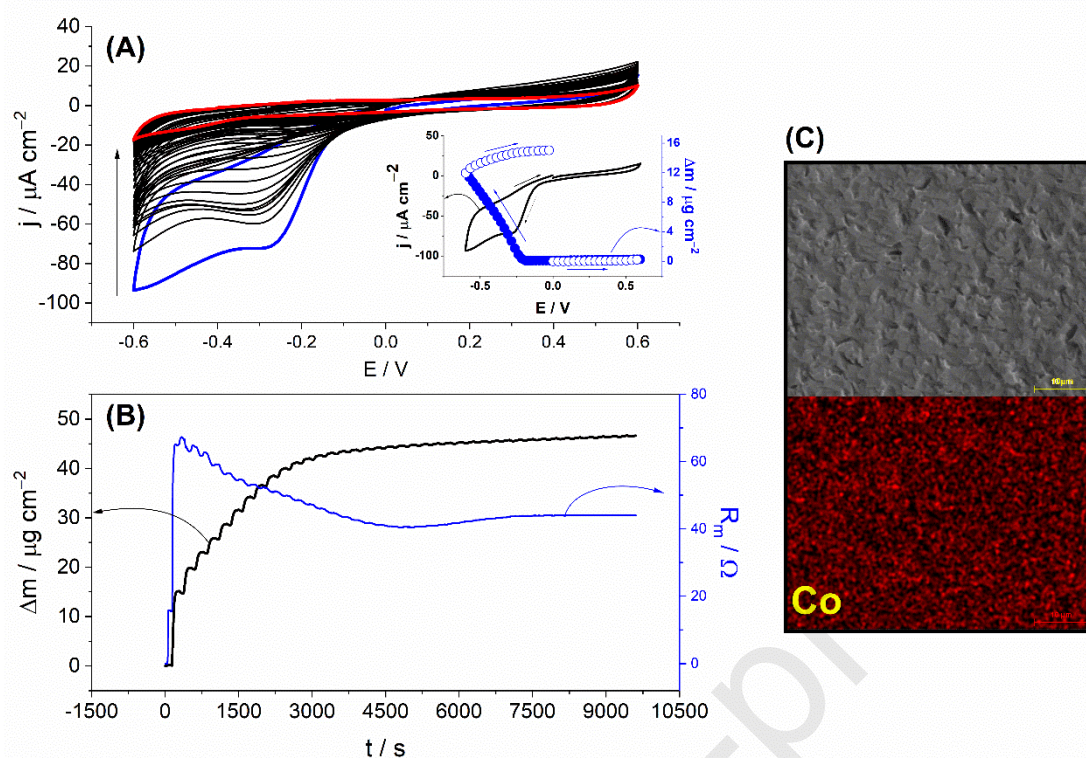
Figure 2. (A) Cobalt insertion in PEDOT by cyclic voltammetry (40 cycles) at 10 mV s^{-1} between 0.6 V to −0.6 V in 0.1M $Co(NO_3)_2$ aqueous solution (blue line is for the first cycle and red line is for the last cycle) to form the PEDOT(Co) (pH=5.1). The inset in (A) shows the mass response during the first cycle; open circles indicate the anodic direction and closed circles the cathodic direction of potential sweep. (B) Mass and motional resistance response with the experimental time. (C) EDX elemental mapping of PEDOT(Co) (Cobalt species are indicated by red colour, scale: $10\mu m$). The auxiliary electrode was a Pt mesh, and the reference electrode was the Ag|AgCl|KCl$_{(sat)}$ electrode which all potentials are referred to (+0.197 V vs SHE at 298 K).

27
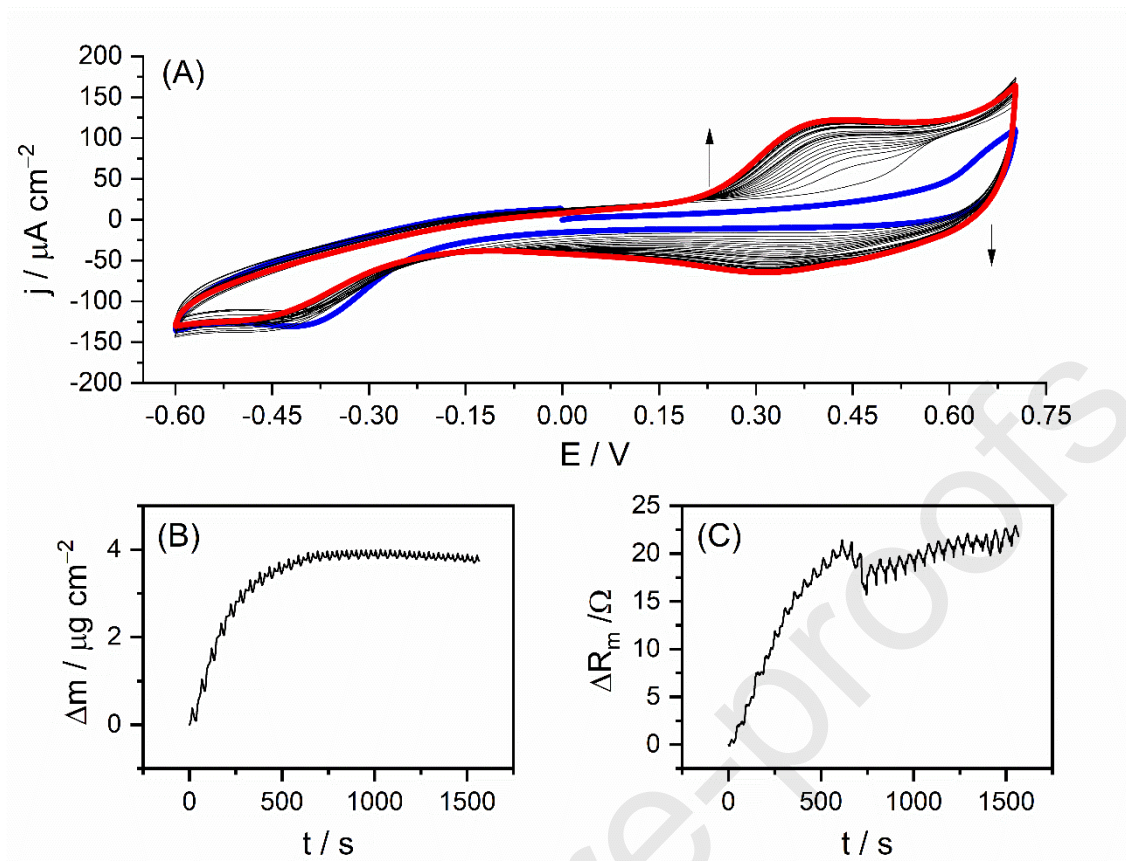
Figure 3. (A) PEDOT(Co) activation by cyclic voltammetry in 0.1M LiClO$_4$ aqueous solution at 10 mV s^{-1} between 0.7 V to –0.6 V (blue line is for the first cycle and red line is for the last cycle) to form PEDOT(aCo) (pH=7.0). (B) Mass response and (C) motional resistance response with the experimental time. The auxiliary electrode was a Pt mesh, and the reference electrode was the Ag|AgCl|KCl(sat) electrode which all potentials are referred to (+0.197 V vs SHE at 298 K).
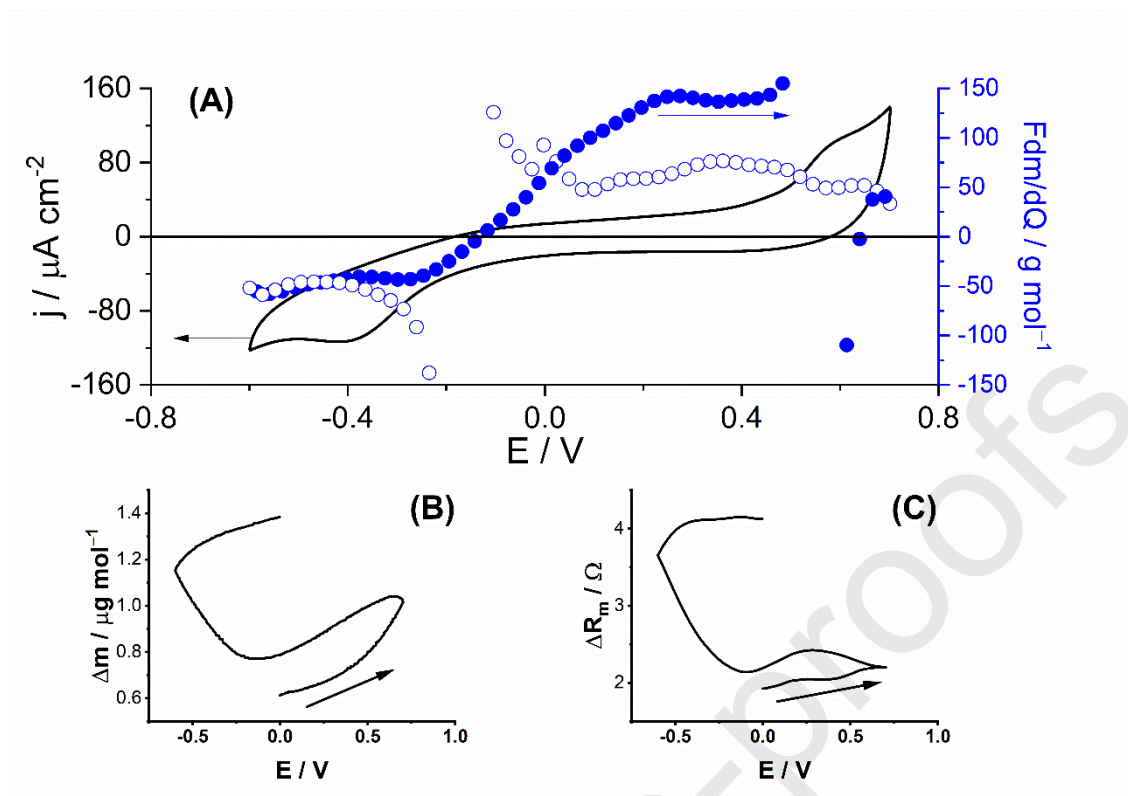
Figure 4. (A) $F(dm/dQ)$ (eq (1)) during the second activation cycle of PEDOT(Co) by cyclic voltammetry in 0.1M LiClO$_4$ aqueous solution at 10 mV s^{-1} between 0.7 V to -0.6 V (pH=7.0). Open circles indicate the anodic direction and closed circles the cathodic direction of potential sweep. (B) the mass and (C) the motional resistance response during this cycle. The arrows in (B) and (C) indicate the beginning and direction of cycle. The auxiliary electrode was a Pt mesh, and the reference electrode was the Ag|AgCl|KCl$_{(sat)}$ electrode which all potentials are referred to (+0.197 V vs SHE at 298 K).
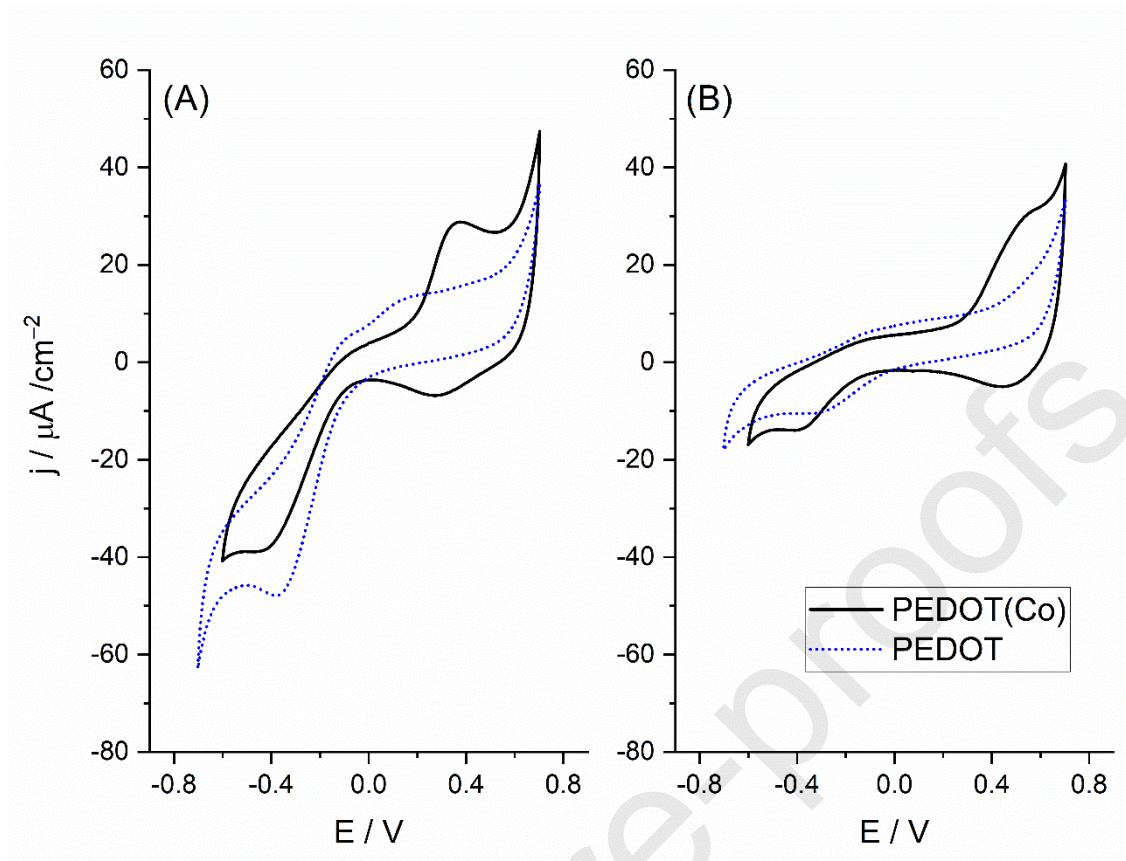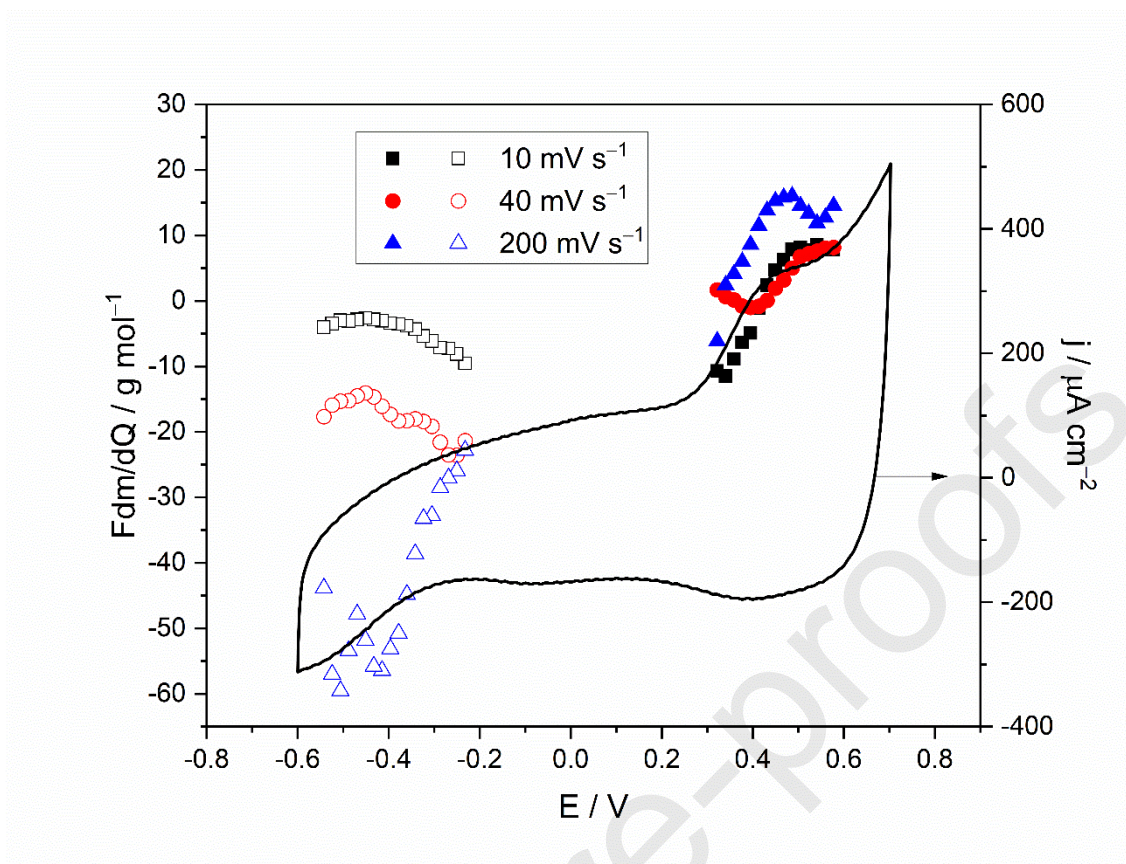
Figure 5. Cyclic voltammetry of PEDOT and PEDOT(aCo) in 0.1M LiClO$_4$ aqueous solution (pH=7.0) at 10 mV s^{-1} between 0.7 V to −0.7 V without argon deaeration (A) and with argon deaeration for 5 min (B).
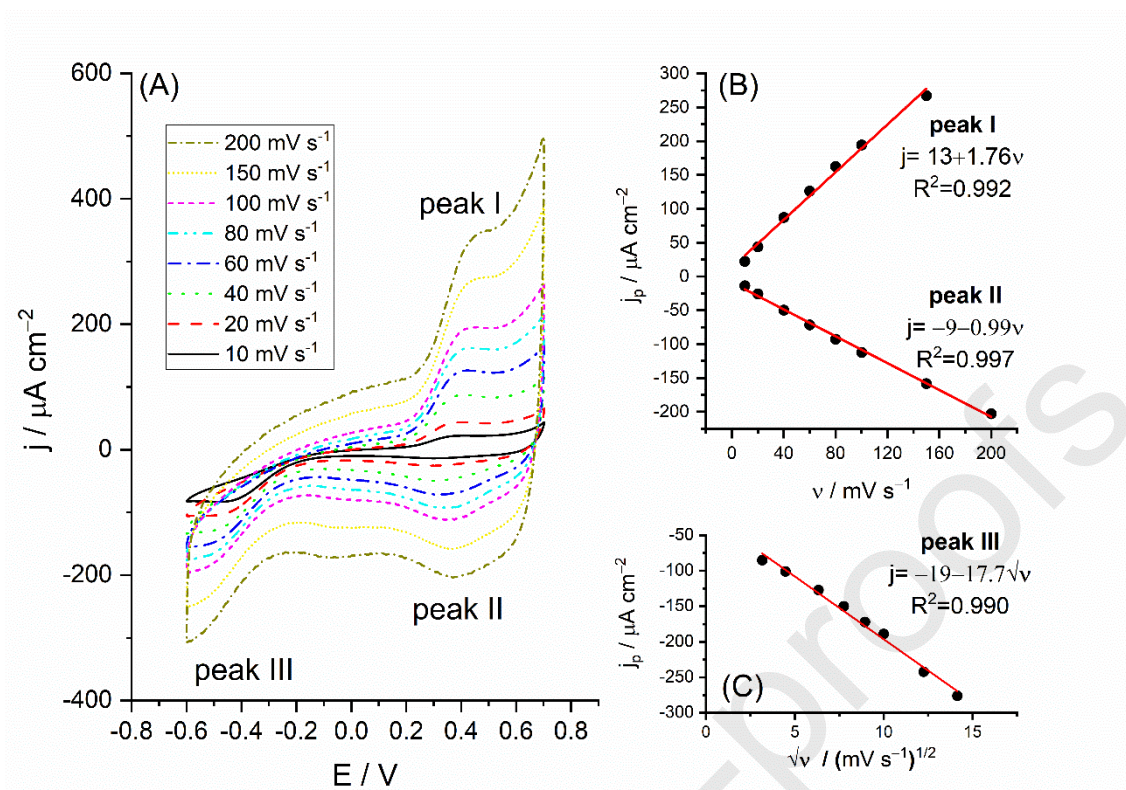
Figure 6. (A) Cyclic voltammetry of PEDOT(aCo) in 0.1M LiClO$_4$ aqueous solution (pH=7.0) at different scan rates between 0.7V and −0.7V without argon deaeration. (B) and (C) is the linear fit analysis of current peaks with the scan rate. The auxiliary electrode was a Pt mesh, and the reference electrode was the Ag|AgCl|KCl(sat) electrode which all potentials are referred to (□0.197 V vs SHE at 298 K).

Figure 7. $F(dm/dQ)$ (eq. (1)) of PEDOT(aCo) by cyclic voltammetry in 0.1M LiClO$_4$ aqueous solution (pH=7.0) at different scan rates and the cyclic voltammogram at 200 mV s^{-1} as visual reference. Open circles indicate the anodic direction and closed circles the cathodic direction of potential sweep. The auxiliary electrode was a Pt mesh, and the reference electrode was the Ag|AgCl|KCl$_{(sat)}$ electrode which all potentials are referred to (+0.197 V vs SHE at 298 K).
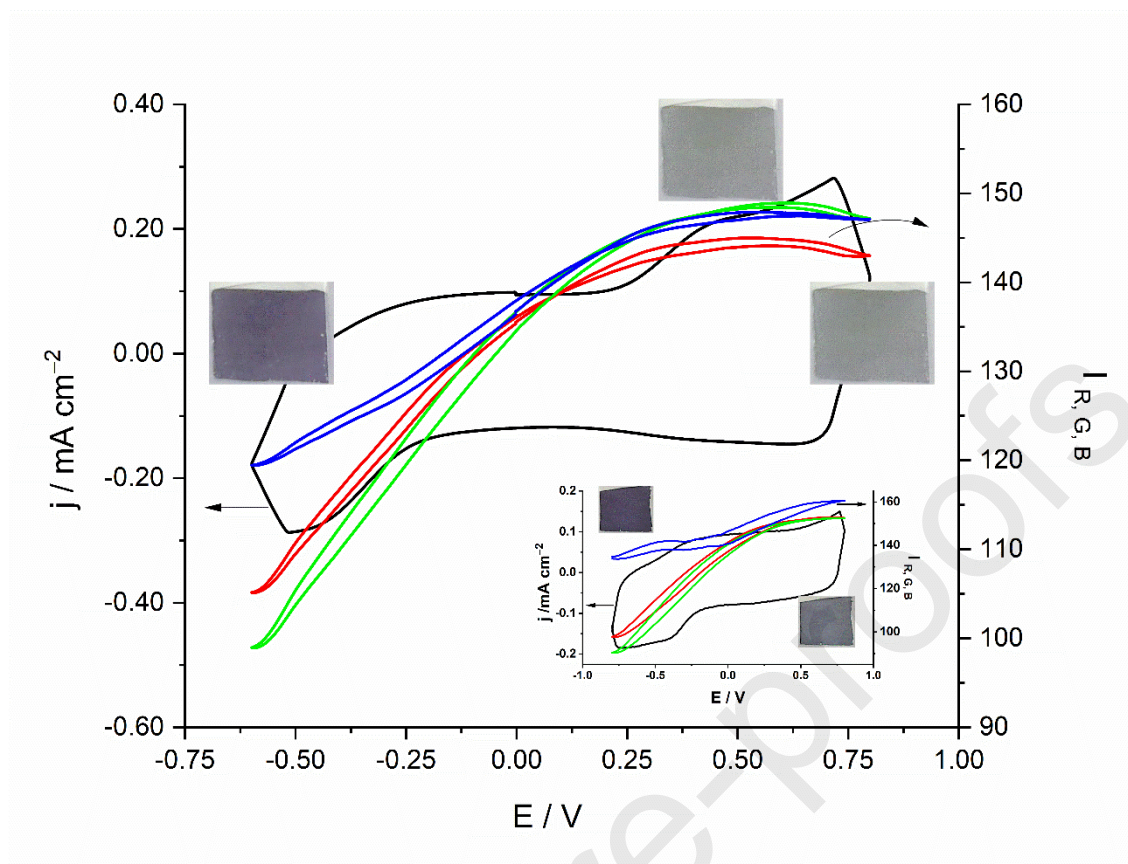
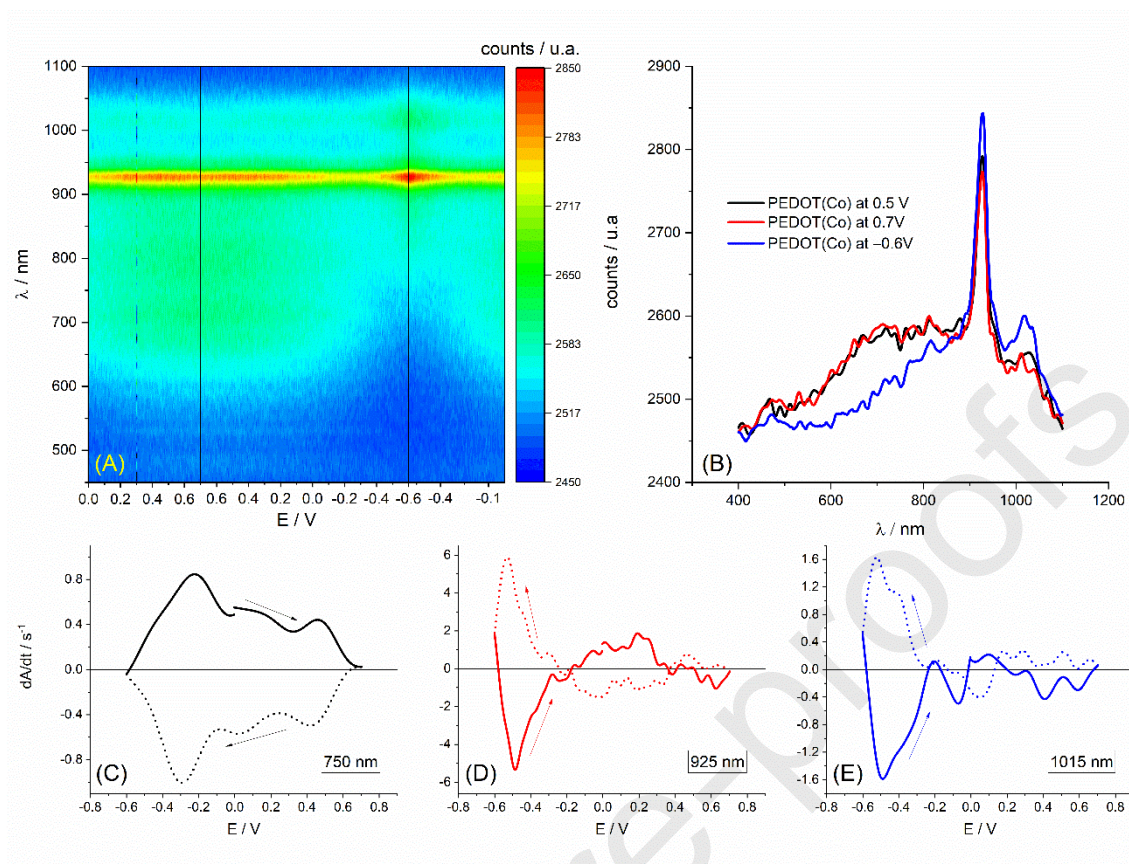Figure 8. DVEC results of PEDOT(aCo) on ITO electrode in 0.1M LiClO$_4$ aqueous solution (pH=7.0) at 100 mV s^{-1}. The inset shows results of PEDOT in identical conditions. The auxiliary electrode was a Pt mesh, and the reference electrode was the Ag|AgCl|KCl$_{(sat)}$ electrode which all potentials are referred to (+0.197 V vs SHE at 298 K).

33

Figure 9. (A) Spectroelectrochemical characterization of PEDOT(aCo) at a scan rate of 10 mV s^{-1} between −0.6 V and 0.7 V in a 0.1 M LiClO$_4$ aqueous solution (pH=7.0). (B) The vis-NIR spectrum of oxidized and reduced PEDOT(aCo) between 450 nm and 1100 nm. (C-E) dA^{λ}/dt vs E at some characteristics wavelengths. The auxiliary electrode was a Pt mesh, and the reference electrode was the Ag|AgCl|KCl$_{(sat)}$ electrode which all potentials are referred to (+0.197 V vs SHE at 298 K).

34
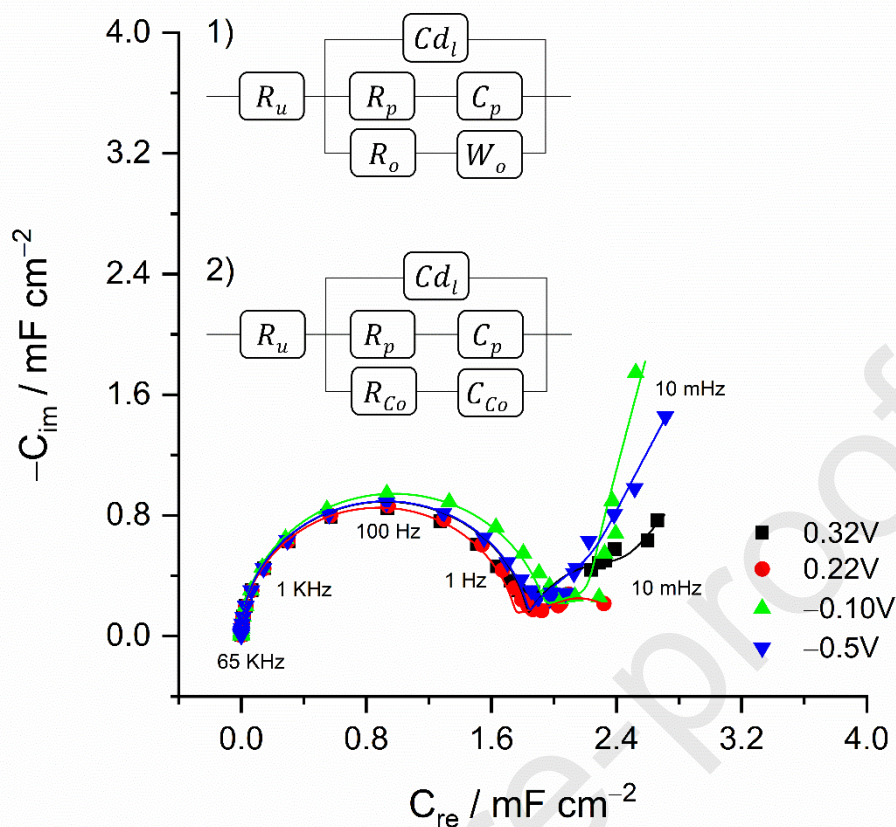
Figure 10. Cole-Cole diagram from the electrochemical impedance spectroscopy of PEDOT(aCo) in a 0.1 M LiClO$_4$ aqueous solution (pH=7.0) at different stabilization potentials. The electrical models used for fittings are included. The dotted representation corresponds to the experimental values and the continuous line to the fittings. Equivalent circuits 1) fitting for the potentials between -0.5V to -0.1V and 2) fitting for 0.22V and 0.32V. The auxiliary electrode was a Pt mesh, and the reference electrode was the Ag|AgCl|KCl$_{(sat)}$ electrode which all potentials are referred to (+0.197 V vs SHE at 298 K).
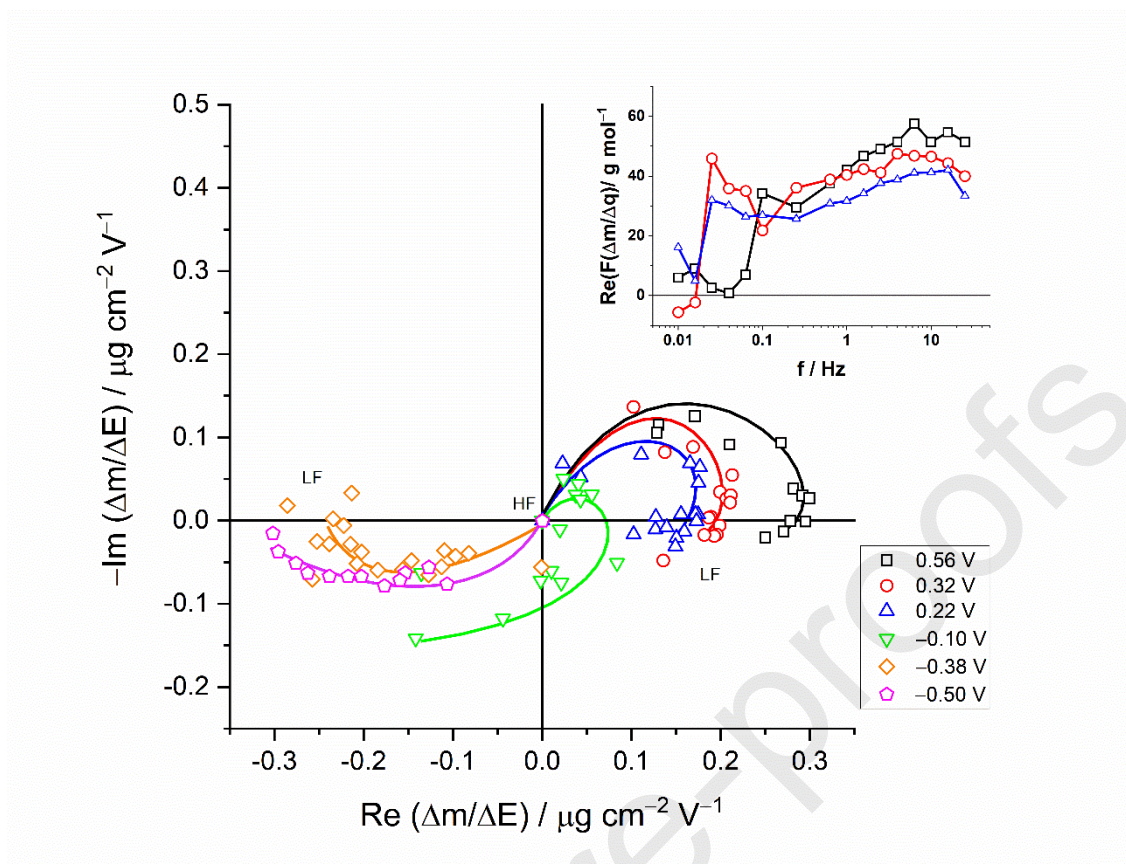
Figure 11. ac-electrogravimetry of PEDOT(aCo) in 0.1M LiClO$_4$ aqueous solutions (pH=7.0) at different potentials. HF and LF indicate high and low frequencies respectively. The inset shows the real part of $F\Delta m/\Delta q(\omega)$ at each frequency for the positive potentials. The auxiliary electrode was a Pt mesh, and the reference electrode was the Ag|AgCl|KCl(sat) electrode which all potentials are referred to ($\square$0.197 V vs SHE at 298 K).
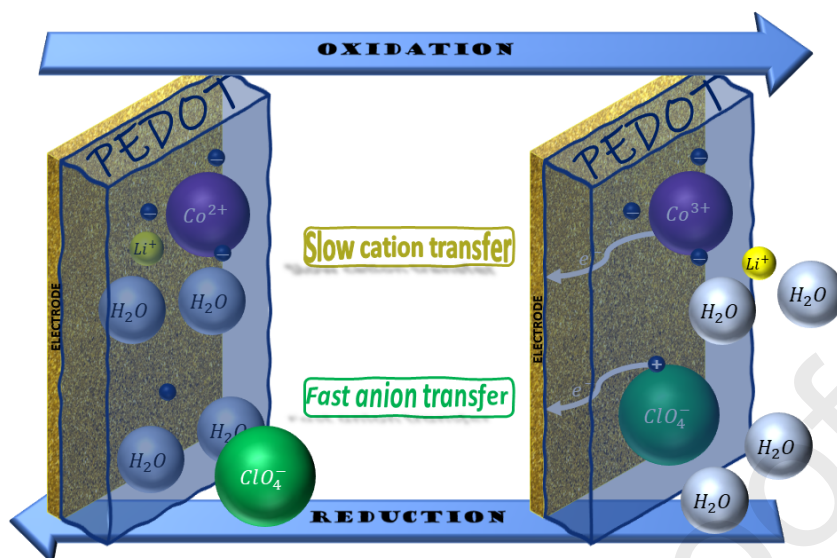
Figure 12. Schematic representation of the proposed electron transfer and doping-dedoping mechanism during the capacitance response of PEDOT(aCo). The smallest spheres inside PEDOT represent fixed charges within the film. Positive charges represent positive polarons and negative charges represent negative polarons and/or nitrate ions.
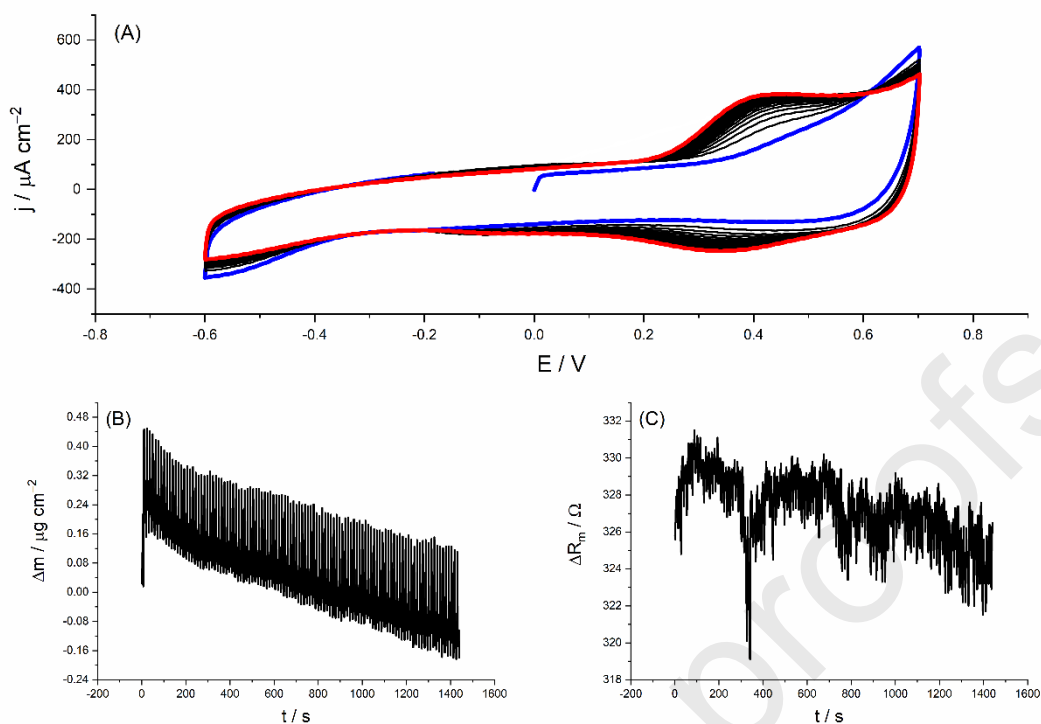
Figure 13. Cyclic stability of PEDOT(aCo). (A) 100 voltammetric cycles at 200mV s^{-1} between -0.6 to 0.7V in 0.1M LiClO$_4$ aqueous solution (pH=7.0). The blue line is for the first cycles and red line is for the last cycle. (B) mass and (C) motional resistance signals. The auxiliary electrode was a Pt mesh, and the reference electrode was the Ag|AgCl|KCl$_{(sat)}$ electrode which all potentials are referred to (+0.197 V vs SHE at 298 K).

38